NASA/TP-1999-209538

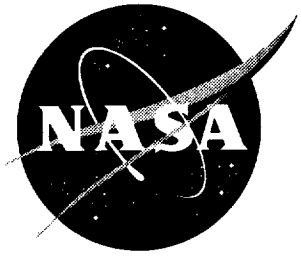

Low-Speed Investigation of Upper-Surface Leading-Edge Blowing on a High-Speed Civil Transport Configuration

Daniel W. Banks, Brenda E. Gile Laflin, Guy T. Kemmerly, and Bryan A. Campbell
Langley Research Center, Hampton, Virginia

December 1999

The NASA STI Program Office . . . in Profile

Since its founding, NASA has been dedicated to the advancement of aeronautics and space science. The NASA Scientific and Technical Information (STI) Program Office plays a key part in helping NASA maintain this important role.

The NASA STI Program Office is operated by Langley Research Center, the lead center for NASA's scientific and technical information. The NASA STI Program Office provides access to the NASA STI Database, the largest collection of aeronautical and space science STI in the world. The Program Office is also NASA's institutional mechanism for disseminating the results of its research and development activities. These results are published by NASA in the NASA STI Report Series, which includes the following report types:

- TECHNICAL PUBLICATION. Reports of completed research or a major significant phase of research that present the results of NASA programs and include extensive data or theoretical analysis. Includes compilations of significant scientific and technical data and information deemed to be of continuing reference value. NASA counterpart of peer-reviewed formal professional papers, but having less stringent limitations on manuscript length and extent of graphic presentations.

- TECHNICAL MEMORANDUM. Scientific and technical findings that are preliminary or of specialized interest, e.g., quick release reports, working papers, and bibliographies that contain minimal annotation. Does not contain extensive analysis.

- CONTRACTOR REPORT. Scientific and technical findings by NASA-sponsored contractors and grantees.

- CONFERENCE PUBLICATION. Collected papers from scientific and technical conferences, symposia, seminars, or other meetings sponsored or co-sponsored by NASA.

- SPECIAL PUBLICATION. Scientific, technical, or historical information from NASA programs, projects, and missions, often concerned with subjects having substantial public interest.

- TECHNICAL TRANSLATION. English-language translations of foreign scientific and technical material pertinent to NASA's mission.

Specialized services that complement the STI Program Office's diverse offerings include creating custom thesauri, building customized databases, organizing and publishing research results . . . even providing videos.

For more information about the NASA STI Program Office, see the following:

- Access the NASA STI Program Home Page at ***http://www.sti.nasa.gov***

- Email your question via the Internet to help@sti.nasa.gov

- Fax your question to the NASA STI Help Desk at (301) 621-0134

- Telephone the NASA STI Help Desk at (301) 621-0390

- Write to:
  NASA STI Help Desk
  NASA Center for AeroSpace Information
  7121 Standard Drive
  Hanover, MD 21076-1320

NASA/TP-1999-209538

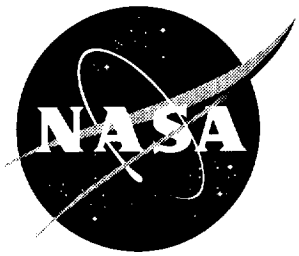

Low-Speed Investigation of Upper-Surface Leading-Edge Blowing on a High-Speed Civil Transport Configuration

Daniel W. Banks, Brenda E. Gile Laflin, Guy T. Kemmerly, and Bryan A. Campbell
Langley Research Center, Hampton, Virginia

National Aeronautics and
Space Administration

Langley Research Center
Hampton, Virginia 23681-2199

December 1999

Available from:

NASA Center for AeroSpace Information (CASI)
7121 Standard Drive
Hanover, MD 21076-1320
(301) 621-0390

National Technical Information Service (NTIS)
5285 Port Royal Road
Springfield, VA 22161-2171
(703) 605-6000

Summary

An exploratory investigation of the effectiveness of upper-surface leading-edge blowing on a High-Speed Civil Transport (HSCT) configuration was conducted in the Langley 14- by 22-Foot Subsonic Tunnel. The objective of the investigation was to determine how effective upper-surface leading-edge blowing is for increasing lift and lift-drag ratios for an HSCT-class airplane at takeoff, initial climb, and approach to landing. The research was conducted on a modified model of a generic HSCT configuration. The model geometry included a cranked delta wing with an inboard sweep of 71°, an outboard sweep of 50°, and a relatively thin airfoil section. Because the leading edge was thin, the blowing slot, unlike conventional leading-edge blowing tangent to the leading edge, was behind the leading-edge and blowing tangent to the upper surface. Furthermore, because of fabrication constraints, the blowing slot was located only on the inboard two-thirds of the wing 71°-sweep leading edge.

Results indicate that upper-surface leading-edge blowing on a highly swept wing with a thin and relatively sharp leading edge, *at the test conditions*, had little effect on increasing lift and lift-drag ratios and, in fact, often decreased these parameters. The upper-surface leading-edge blowing appeared to affect the local flow structure, but it did not have the beneficial effect on the overall lift and drag as had been predicted by a preliminary analytical study. *However, this investigation covered a limited parameter space and does not attest to the effectiveness possible with other geometries and conditions.*

Introduction

There has been significant recent interest in developing the technologies needed for an efficient and environmentally friendly next-generation supersonic transport. An area of great concern for this High-Speed Civil Transport (HSCT) is the acoustic impact on the community living under the flight path of these airplanes during takeoff and initial low-altitude climb. Typically an airplane of the size envisioned would emit significant noise from the engines operating at high power settings during the early stages of flight. Also, because this airplane is designed for high-speed cruise, it has, by nature, relatively poor low-speed performance and thus relatively high thrust requirements for takeoff and high speeds on approach. Many ideas and scenarios have been developed to reduce the undesirable noise. Engine manufacturers have strived to produce quieter and more efficient engines, reduced-thrust takeoff procedures have been developed, and high-lift systems are being developed that would either enable the airplane to climb to a higher altitude faster or allow a similar flight path with reduced thrust. Conventional high-lift systems usually consist of a combination of leading- and trailing-edge flap systems to provide increased lift-drag ratio L/D for takeoff and lift coefficient C_L for approach. These flap systems function effectively, but their added weight and complexity detract from the higher speed cruise efficiency of the airplane.

Some innovative systems have been conceived to improve the low-speed flight performance and to have minimal impact on cruise performance. One idea that has been investigated recently employed leading-edge suction (ref. 1) for boundary layer control and vortex suppression to alleviate the pitch-up that limits the trimmable angle-of-attack range and subsequent usable maximum lift coefficient. The system comprised a porous section covering the entire leading edge from the lower to the upper surface over the inboard span of the wing and a suction device that would suck off the boundary layer and suppress the leading-edge vortex. This system permitted a higher trimmed angle-of-attack range because of the increased angle of attack where pitch-up occurs. Therefore, higher trimmed maximum lift coefficients at takeoff and climb were possible. The major components of the suction system were anticipated to be developed and readily available should a proposed hybrid laminar flow system be used for cruise drag reduction. One disadvantage of the system is its susceptibility to insects, rain, snow, and ice clogging the suction ports and making them ineffective.

Similar benefits could possibly be obtained with leading-edge blowing systems without the disadvantages of the suction system. Other potential benefits that result from a blowing system include automatic anti-icing (direct engine bleed air is relatively hot) as well as airplane lateral control. Several analytical studies and experimental investigations have been conducted into the potential benefits of leading-edge blowing on delta wing configurations; some are listed in references 2–6. Because the geometry of the proposed HSCT configuration at the time of this study had a relatively thin wing section with a small leading-edge radius, conventional leading-edge blowing concepts were not feasible. Conventional concepts are typically applicable to a thicker wing section with a larger leading-edge radius and blowing from the apex of and tangent to the leading edge. The high curvature of the leading edge augments the jet entrainment inducing a strong flow acceleration and suction, thereby delaying leading-edge separation, which increases maximum lift and lift-drag ratio. However, significant benefits to lift and lift-drag ratio were predicted in a preliminary analytical study of a delta wing with the blowing slot on the upper surface just aft of the leading edge that directed blowing normal to the leading edge and tangent to the upper surface; the wing had a

relatively thin, sharp leading-edge section similar to the aforementioned HSCT section. Both upper-surface leading-edge blowing and conventional leading-edge blowing concepts are shown in figure 1. The mechanism, which the upper-surface leading-edge blowing uses to produce increased lift and lift-drag ratios, is similar to that of conventional methods except for the location at the leading-edge region. The study indicated that the jet in this region at lower blowing rates would reduce the strength of the primary vortex and increase the leading-edge suction, thereby increasing the lift-drag ratio. At higher blowing rates, the primary vortex strength and location appeared to be appreciably influenced and gains in maximum attainable lift as well as lift-drag ratio similar to those for conventional leading-edge blowing could be realized. Although not as beneficial as conventional leading-edge blowing because of the reduced effectiveness on the leading edge, significant improvement appeared to be possible.

An investigation of an upper-surface leading-edge blowing system has been conducted in the Langley 14- by 22-Foot Subsonic Tunnel. The objective was to determine if such a system could produce the desired improvements in lift and lift-drag ratio on this class of aircraft. The research was conducted by modifying an existing model of a generic HSCT configuration. The model geometry included a cranked delta wing with an inboard sweep of 71°, an outboard sweep of 50°, and a relatively thin airfoil. The model was truncated forward of the empennage and, therefore, did not have vertical or horizontal tail surfaces; as such, it did not represent a trimmed configuration. The blowing slot, unlike conventional leading-edge blowing geometries, was located just downstream of the leading edge and directed blowing tangent to the upper surface; it was not located on and blowing up and tangent to the leading edge. Furthermore, because of fabrication constraints, the blowing slot was located only on the inboard two-thirds of the wing 71°-sweep leading edge. Data were obtained for the cruise wing (flaps undeflected), high-lift wing (flaps deflected to takeoff settings except for the inboard leading-edge section), and the high-lift wing with a leading-edge Krueger flap ahead of the blowing slot. Data were obtained across an angle-of-attack range from −2° to 26°, a dynamic pressure range from 20 psf to 70 psf, which corresponds to a Mach number range of 0.12 to 0.22, and at blowing-momentum coefficients up to approximately 0.1. The Reynolds number, which was based on the mean aerodynamic chord, ranged from 2.5×10^6 to 4.5×10^6. Results from the investigation show that this blowing method, *at the test conditions*, did not provide any significant beneficial effects as had been predicted by a previous analytical study. *However, this investigation covered a limited parameter space and does not attest to the effectiveness possible with other geometries and conditions.*

Symbols

a	speed of sound, ft/sec
C_D	drag coefficient, $\frac{\text{Drag}}{q_\infty S}$
C_L	lift coefficient, $\frac{\text{Lift}}{q_\infty S}$
C_m	pitching-moment coefficient, $\frac{\text{Pitching moment}}{q_\infty S\bar{c}}$
C_p	pressure coefficient, $\frac{p - p_\infty}{q_\infty}$
C_μ	blowing-momentum coefficient, $\frac{\dot{m}V_j}{q_\infty S}$
$\bar{c}$	mean aerodynamic chord, ft
L/D	lift-drag ratio, $\frac{C_L}{C_D}$
L/D_{eq}	equivalent lift-drag ratio, $\frac{C_L}{C_D + C_\mu}$
L/D_{max}	maximum lift-drag ratio
M	Mach number, $\frac{V_\infty}{a}$
$\dot{m}$	blowing mass flow rate, slug/sec
p	local static pressure, psf
p_∞	free-stream static pressure, psf
q_∞	free-stream dynamic pressure, psf
R	Reynolds number based on mean aerodynamic chord, $\frac{\rho_\infty V_\infty \bar{c}}{\mu}$
S	wing reference area, ft^2
V_j	jet exit velocity, ft/sec
V_∞	free-stream velocity, ft/sec
x/c	nondimensional chord location, $\frac{\text{Local distance}}{\text{Local chord}}$
α	angle of attack, deg
δ	flap deflection angle, normal to hinge line (positive down), deg
μ	viscosity, lb-sec/ft^2
ρ_∞	free-stream density, slug/ft^3

Subscripts:

eq	equivalent
LE, i	leading edge inboard

LE, *o* leading edge outboard

TE, *i* trailing edge inboard

TE, *o* trailing edge outboard

Abbreviations:

BL model butt line, in.

FS model fuselage station, in.

HSCT High-Speed Civil Transport

WL waterline, in.

Model Description

Wind Tunnel Model

A photograph and sketches of the model, as tested in this investigation, are presented in figure 2. The wing has an inboard sweep of 71° and an outboard sweep of 50° with no twist or camber. The flap systems consist of leading-edge flap segments and partial span trailing-edge flap segments spaced to accommodate engine nacelle placement, although no nacelles were present. The two most-inboard flap segments on each side were always deflected together at the same angle and were jointly referred to as the inboard trailing-edge flaps.

Tests were conducted on three configurations. The first was the cruise wing with all leading- and trailing-edge flaps undeflected. The cruise wing was tested as a baseline to determine the effects of the leading-edge blowing without deflected surfaces and not to assess the usefulness of blowing at cruise flight conditions. The second was the high-lift wing with leading- and trailing-edge flaps deflected as would be expected for takeoff, with the exception that the inboard leading edge could not be deflected because of presence of the blowing system. Deflections were 26.4° for the outboard leading-edge flap, 12.8° for the outboard trailing-edge flap, and 10° for the inboard trailing-edge flap. The third configuration was the high-lift wing with the Krueger flap, which was identical to the high-lift wing except for the Krueger flap (fig. 2(c)) attached to the entire length of the wing 71°-sweep leading edge. The Krueger flap was assumed to allow attached flows at higher angles of attack, and the blowing would occur approximately at the hinge line, which could potentially eliminate hinge-line separation. The model had no canards, tail surfaces, or engine nacelles. The model is truncated forward of the empennage section where the horizontal and vertical control surfaces would normally be located, and the data do not represent a complete or trimmed configuration. The left wing of the model was plumbed to measure numerous surface pressures. The geometric details of the model are presented in table I.

Transition grit (No. 60) was applied to both the forebody (fig. 2(d)) and the wing upper-surface flap leading edges (outboard leading-edge flaps and Krueger flaps) at 5-percent local chord to fix boundary layer transition from laminar to turbulent flow at attached flow conditions. Grit was not applied in the region of the blowing slots.

Blowing System

The blowing system consisted of a slot located on the inboard swept portion of each wing. A close-up photograph of the leading-edge blowing slots and schematic drawings of the blowing system are shown in figure 3. The slot consisted of 23 segments with a structural bridge between each. These structural bridges also served as flow fences, which kept the jet exit flow normal to the leading edge and evenly mixed along the length of the slot. The slots were nominally 0.015 in. high by 0.875 in. wide, and the bridge between them was 0.25 in. wide. (See fig. 3(e).) Pressurized air was supplied from a plenum located behind the slot in the wing leading edge. The plenum was connected to the air supply system by a pair of 3/8-in.-diameter stainless steel tubes that bridged the balance. The supply air mass flow was measured with a system venturi mass flow meter. The slots directed blowing aft with the flow tangent to the upper surface in a direction normal to the leading edge.

Test Conditions and Instrumentation

The investigation was conducted in the Langley 14- by 22-Foot Subsonic Tunnel. A description of the tunnel and associated hardware can be found in reference 7. Test Mach numbers M, dynamic pressures q_∞, and Reynolds numbers R based on the wing mean aerodynamic chord $\bar{c}$ were as follows:

M	q_∞, psf	R
0.12	20	2.50×10^6
.16	35	3.30
.22	70	4.50

Tests were primarily conducted at zero sideslip across an angle-of-attack range from −2° to 26°.

A six-component strain-gage balance mounted inside the fuselage measured the forces and moments and is shown in figure 4. Tare loads induced by the blowing system that bridged the balance were computed experimentally with known weights applied to the balance–airline system prior to the wind-on test runs and were subtracted from the balance data during the test. Similarly,

the pressure tare loads were also computed experimentally with known pressure loads applied to the capped-air-line–balance system prior to the wind-on test runs and were subtracted from the balance data. The momentum tare loads were small, when compared with the mechanical and pressure loads, and were neglected. The angle of attack was measured by an accelerometer installed in the model. The angle of sideslip was measured by a digital encoder mounted to the turntable drive mechanism of the model support system.

The data were corrected for jet boundary and blockage effects according to the methods of references 8 and 9. An accurate assessment of flow angularity (determined by testing the model both upright and inverted) was not possible due to the nonstandard support system and the presence of the blowing system. However, because only incremental data were necessary for this investigation, no corrections were made for flow angularity or local support system flow interference.

In addition to force and moment data, surface pressure measurements and oil flow visualization were obtained at some conditions. The surface pressure measurements were taken on the upper surface of the left wing, while the oil flow visualization was taken on the right wing. The locations of the pressure orifices are shown in figure 5. The pressures were measured with electronically scanned pressure (ESP) modules. The surface flow visualizations were obtained with a mixture of titanium dioxide (TiO_2) powder (white), mineral oil, and a small amount of oleic acid used as a dispersant. The mixture was applied to the model right wing, which had been painted black for maximum contrast. The model attitude was set, and then the tunnel dynamic pressure and model blowing rate were brought to the desired condition long enough for the oil mixture to set and stabilize. The tunnel dynamic pressure and model blowing rate were then rapidly brought to zero, and photographs were taken. Because of time limitations, the surface flow visualizations were conducted at 4° and 10° angles of attack at selected blowing coefficients. A 10° angle of attack represents the approximate condition for the expected takeoff lift coefficient of approximately 0.4 to 0.5, while a 4° angle of attack represents the approximate angle of attack of the maximum lift-drag ratio of the configurations tested. These were the conditions of greatest interest. Also, flow visualizations were obtained at moderate blowing coefficients, because the highest blowing coefficients were felt to be unrealistic in terms of what flow would be available from engine bleed air.

Presentation of Data

The data used in the analysis of the upper-surface leading-edge blowing concept are presented here. Force and moment data are presented at each test dynamic pressure for both thrust included and thrust removed. Surface flow visualization photographs obtained at selected conditions and the associated pressure distributions are presented as follows:

Results and Discussion

The results of this investigation are presented and discussed. The longitudinal force and moment results are shown in two formats: thrust removed and thrust included. The thrust-removed data have been adjusted for the static thrust components, which were determined from wind-off–jet-on test runs. These data, therefore, show only induced effects and no direct thrust effects. Note that the static thrust forces and moments may not perfectly represent the wind-on thrust effects because the wind-on and wind-off downstream conditions of the nozzle exit may not be identical; however, these results should be reasonably close. The thrust-included data contain all the direct thrust effects. Because of the direct thrust component in the axial direction, drag becomes small and eventually negative at greater blowing rates, so the lift-drag ratio becomes undefined at these conditions. For the thrust-included data, an equivalent lift-drag ratio L/D_{eq} was calculated that added the blowing momentum to the thrust-included drag. (See refs. 10 and 11.) This parameter gives a relative indication of the benefit or penalty including the momentum expended because of blowing.

The cruise and high-lift wing configurations were run at free-stream dynamic pressures of 70, 35, and 20 psf. The high-lift wing configuration with the Krueger flap was run at free-stream dynamic pressures of 20 and 35 psf because the simple construction of the Krueger flaps prohibited higher loads. The purpose of the lower dynamic pressure runs was to increase the blowing-momentum coefficient because the air mass flow to the leading edges was limited. This resulted in maximum blowing-momentum coefficients of approximately 0.03 at 70 psf, 0.06 at 35 psf, and 0.1 at 20 psf.

Cruise Wing Configuration

The longitudinal force and moment results for the cruise wing configuration with thrust removed are presented in figures 6–8. The induced effects at q_∞ = 70 psf (fig. 6) show no significant changes in C_L and C_D with an increasing C_μ. Small increases in L/D occurred near L/D_{max} ($C_L \approx 0.2$) at the lower C_μ with no change at the higher C_μ. A slight stabilizing rotation of the C_m curve about $\alpha \approx 10°$ was noted with an increasing C_μ. The rotation caused a slight decrease in pitching moment below $\alpha \approx 10°$ and a slight increase in C_m above $\alpha \approx 10°$. These trends are probably due to a slight increase in leading-edge suction at low angles of attack and a slight decrease in primary vortex strength at higher angles of attack. However, significant benefits to L/D and C_L, as had been predicted by a previous analytical study, did not result. A slight increase in L/D_{max} of nearly 1 occurred at $C_L \approx 0.2$; no change was noted at takeoff and climb conditions at $C_L \approx 0.4$ to 0.6. At a free-stream dynamic pressure of 35 psf (fig. 7), the trends were similar, but more pronounced, due to a higher C_μ. A very small increase in C_L resulted at angles of attack up to 14° at the higher C_μ, and slightly larger pitching-moment changes resulted with increases in C_μ. However, the net result was a small increase in L/D near $C_L \approx 0.2$ but small or negligible changes at $C_L \approx 0.6$ and greater. The rotation of the C_m curve seemed to be centered about $\alpha \approx 14°$, and the increases at lower angles of attack were greater than the losses at higher angles of attack. This indicates that the increase in leading-edge suction at low angles of attack

was greater than the vortex dissipation at higher angles of attack. At a free-stream dynamic pressure of 20 psf (fig. 8), the trends were similar to those seen at 35 psf, but again the levels were higher due to the higher C_μ at the lower dynamic pressure. Even at the highest C_μ the blowing jet had surprisingly little effect on C_L and L/D, which again was the expected result and desired effect on the flow field.

The results for the cruise wing configuration with thrust included are presented in figures 9–11. At a free-stream dynamic pressure of 70 psf (fig. 9), no significant changes resulted in C_L up to the highest angles of attack. Small reductions in C_D, as would be expected because of the direct thrust component, were most noticeable at the lower angles of attack. However, these reductions in C_D were much smaller than would have been anticipated, even with consideration of the side force cancellation due to the high-sweep angle. Again, a rotation of the C_m curve was seen with the thrust-removed data; however, here the curve appears to have rotated about $\alpha \approx 0°$ with a resultant reduction in C_m with an increasing C_μ and increasing angle of attack. This reduction in pitching moment with an increasing C_μ occurred because the jet lower surface is constrained by the wing and allowed to expand above; therefore, the thrust vector is rotated slightly upward, which causes the nose-down increment with an increasing C_μ. Large reductions in L/D_{eq} were most apparent from $C_L \approx 0.2$ to 0.4. Recall that L/D_{eq} is computed by taking into account the momentum expended in the blowing jet on the decreased drag, and because of the highly swept leading edge, much of this momentum is not recovered. This is due in part to the fact that the slot is swept 71° from the free stream; therefore, much of the thrust component from each side is in the side force direction and cancels each other. At 35 psf (fig. 10) the trends are similar, but the levels are increased; however, now both a rotation and a downward translation of the C_m curve occurred. Also the decrease in L/D_{eq} persists to higher values of C_L. At 20 psf (fig. 11) the trends were again similar to those of 35 psf, but again the levels were higher, and the values of L/D_{eq} were further depressed for higher C_L and C_μ. Also with a higher C_μ, the rotation of the thrust vector that contributed to the nose-down pitching moment also results in small losses in lift.

Surface flow visualizations obtained at a 4° angle of attack at $C_\mu = 0$ and 0.050 at $q_\infty = 20$ psf are shown in figures 12 and 13, respectively. The pressure distributions for the cruise wing at $\alpha = 4°$ and $q_\infty = 20$ psf are shown in figure 14. The results of a 4° angle of attack and $C_\mu = 0.050$ data (fig. 13), when compared with $C_\mu = 0$ data (fig. 12), show a large change of the inboard surface flow from the leading edge to the fuselage junction, which resulted from blowing. The flow starts normal to the swept leading edge and then curves streamwise somewhat before reaching the fuselage junction. Flow outboard of the blowing slots, including the outboard crank, appears to be relatively unaffected. The pressure distributions for this configuration at a 4° angle of attack (fig. 14) show little changes to the wing pressures with blowing at these conditions. This indicates that, although the inboard surface streamlines seemed to be affected by the blowing, the overall pressure distribution and forces and moments were relatively unaffected by blowing at these conditions.

Surface flow visualizations obtained at a 10° angle of attack at $C_\mu = 0$, 0.023, 0.050, and 0.072 at $q_\infty = 20$ psf are shown in figures 15–18. The pressure distributions for the cruise wing at $\alpha = 10°$ and $q_\infty = 20$ psf are shown in figure 19. At a 10° angle of attack, the comparison of $C_\mu = 0.023$ data (fig. 16) with $C_\mu = 0$ data (fig. 15) shows that the forward blowing slots energize the flow again from the leading edge to the fuselage junction, but the rear slot flow appears to be quickly entrained in the primary vortex flow and moves back toward the leading edge and eventually becomes entrained in what appears to be the secondary separation farther downstream. The flow line formed by pooling of the oil mixture roughly parallel to the leading edge indicates a secondary separation of the main vortex flow. As this secondary vortex separation line moves closer to the leading edge and farther downstream, it moves farther outboard with increasing blowing. This would indicate that the upper-surface blowing, which is against the sense of the primary vortex on the surface, is reducing the effect of the vortex on the surface and, therefore, the strength of the secondary separation and vortex. Blowing does not appear to move the primary vortex inboard but just reduces its strength. Also, no increases in leading-edge suction were indicated. Again at a 10° angle of attack but at $C_\mu = 0.050$ (fig. 17), the rear slots, in addition to the forward slots, are now more effective in moving the flow inboard, and the secondary separation line has moved significantly outboard and is not very evident on the main wing. The flow on the outboard crank has changed significantly and is now much more spanwise. An increase in blowing to $C_\mu = 0.072$ (fig. 18) has much the same effect as $C_\mu = 0.050$ but is more accentuated because of the greater blowing rate.

The effect of blowing on pressure distributions (fig. 19) is most noticeable at the outboard crank station where there is a reduction in the maximum suction from $C_p \approx -1.0$ at $C_\mu = 0$ to $C_p \approx -0.5$ at $C_\mu = 0.072$ A small increase in maximum suction occurred at the inboard crank station with little change elsewhere. This is an indication of the effect of the secondary vortex flow on the crank, which has now been diminished. Although the outboard crank is the only location showing a significant

effect on pressure distribution due to blowing, it is not the major contributor to the changes in the force and moment data due to blowing. This is evident by the fact that the suction on the outboard crank is decreasing with increasing blowing and is behind the moment reference center; yet, a nose-down increment occurs with blowing (thrust-included data).

High-Lift Wing Configuration

The longitudinal force and moment results for the high-lift wing configuration with thrust removed are presented in figures 20–22. The characteristics without blowing are very similar (i.e., no large increase in C_L or L/D) to those of the cruise wing configuration. This is due in part to not having the deflected leading-edge flap on the main wing (because of the blowing slot) and the ineffectiveness of the trailing-edge flaps alone. With blowing in general, the trends seen with the high-lift wing configuration are similar to those seen with the cruise wing configuration. At a free-stream dynamic pressure of 70 psf (fig. 20), small, relatively insignificant changes in C_L and C_D resulted from an increasing C_μ. Small reductions in L/D occurred near $C_L \approx 0.2$ and almost no change between $C_L \approx 0.4$ to 0.6. As seen with the cruise wing configuration, a rotation of the C_m curve around $\alpha \approx 10°$ resulted. Once again the trends at $q_\infty = 35$ (fig. 21) and 20 psf (fig. 22) were similar to those at 70 psf, with the levels being greater as expected because C_μ is also increasing. Also, greater losses in L/D occurred at the highest blowing rates. At 20 psf, L/D increased slightly at $C_\mu = 0.05$ and $C_L \approx 0.2$ to 0.4.

The results for the high-lift wing configuration with thrust included are presented in figures 23–25. The thrust-included data essentially show the same trends as seen in the thrust-included data for the cruise wing configuration, except that the losses in L/D_{eq}, with blowing are much greater for the high-lift wing configuration. The general trends are a decrease in C_L, a decrease in C_D, a downward rotation and translation of the C_m curve, and a reduction in L/D_{eq}, all with an increasing C_μ. This decrease in C_L and L/D with increasing blowing is an unexpected and detrimental effect.

Surface flow visualization for the high-lift wing is shown in figures 26–30; pressure distributions are shown in figures 31 and 32. All results for the high-lift wing were at an angle of attack of 10° but at dynamic pressures of 35 and 20 psf. Comparison of the results for $C_\mu = 0.015$ and $q_\infty = 35$ psf (fig. 28) with the unblown results at the same dynamic pressure (fig. 26) shows that the forward slots energize the flow from the leading edge to the fuselage juncture but that the flow from the rear section of the slot is quickly entrained into the primary vortex flow. The secondary separation is moved closer to the leading edge, which indicates that the primary vortex has been weakened, but the flow outboard on the crank region looks relatively unaffected. With dynamic pressure reduced to 20 psf, results for $C_\mu = 0.025$ (fig. 29) compared with $C_\mu = 0$ and $q_\infty = 20$ psf (fig. 27) are similar, but the higher blowing rate moves more flow inboard and more slots located farther aft are effective; this occurs before the flow is entrained into the primary vortex flow. Movement of the secondary separation line and the effect on the crank region are also similar to those for the previous condition. These are consistent with the results obtained at the same angle of attack with the cruise wing, which is not surprising because the leading edge of the main wing is the same. At $C_\mu = 0.050$ (fig. 30) the rear slots are now more effective, as expected; however, the crank section is still not significantly affected, which is probably due to the more attached nature of the flow on the crank with the outboard leading-edge flap deflected as shown in the pressure distributions in figures 31 and 32. The cruise wing had a greater change in pressure distribution on the outboard crank station. For the cruise wing (fig. 19), the outboard crank station was the only location to show a definite and significant trend. However, except for the front three ports at the highest blowing rate (fig. 32), this location for the high-lift wing shows little, if any, effect from blowing.

High-Lift Wing Configuration With Krueger Flap

The longitudinal force and moment results for the high-lift wing configuration with the Krueger flap with thrust removed are presented in figures 33 and 34. This configuration was only run at 35 and 20 psf dynamic pressures because the simple construction of the Krueger flaps limited load capability. This configuration followed most of the same trends as were seen on the cruise and high-lift wing configurations. Without blowing, this configuration was very similar to the high-lift wing configuration in all respects. This configuration seemed to be less sensitive to blowing and blowing rate than the other two configurations, as shown by the smaller changes with an increasing C_μ. This is most likely due to the more attached nature of the flow with the Krueger flap leading edge and, therefore, less vortex flow field to effect. At $q_\infty = 35$ psf the pitching-moment curve appears to have rotated about $\alpha \approx 18°$. Virtually no change in L/D occurred except for the highest C_μ; $C_\mu = 0.056$ at $q_\infty = 35$ psf and $C_\mu = 0.099$ at 20 psf. Also, C_L increased slightly at $q_\infty = 35$ psf up to $\alpha \approx 14°$ (fig. 33) and decreased slightly at $\alpha > 14°$. Again, C_L increased slightly at $q_\infty = 20$ psf for $\alpha \approx 14°$ to 22° (fig. 34) and decreased slightly at $\alpha > 22°$. Because blowing had no observed beneficial effect on this configuration, it most

likely did not have the anticipated significant effect on reducing hinge-line separation on the lee side of the Krueger flap.

The results for the high-lift wing configuration with the Krueger flap with thrust included are presented in figures 35 and 36. Once again the trends displayed by this configuration are similar to those seen on the cruise and high-lift wing configurations. The values of C_L and C_m were somewhat smaller than those seen on the high-lift wing configuration and, again, were most likely due to the more attached nature of the flow on the main wing.

The results for the surface flow visualization for the high-lift wing with the Krueger flap are presented in figures 37–39, and the respective pressure distributions are shown in figure 40. In addition to the $C_\mu = 0$ test (fig. 37), both blowing conditions are shown for a 10° angle of attack at $q_\infty = 20$ psf. At $C_\mu = 0.026$ (fig. 38) most of the slots appear to be energizing the flow inboard to the fuselage junction. This is different from the cruise (fig. 13) and high-lift (fig. 30) wings. However, this would be expected because, with the Krueger flap, the main wing flow should be more attached and in a streamwise direction, and the blowing is not working against the primary vortex flow back toward the leading edge. The crank flow also looks much the same as with no blowing and is similar to what was seen with the high-lift wing. This indicates the streamwise and less interactive nature of the flow with the high-lift wing and the Krueger flap. At $C_\mu = 0.050$ (fig. 39) the flow appears to be more energized inboard, as expected; however, the crank flow looks similar to $C_\mu = 0.026$. In general, the pressure distributions (fig. 40) show a slight depression of the suction level on the crank with blowing and no discernible differences at the midstation or inboard stations.

Conclusions

An exploratory investigation of the effectiveness of upper-surface leading-edge blowing on an High-Speed Civil Transport (HSCT) configuration was conducted in the Langley 14- by 22-Foot Subsonic Tunnel. The objective of the test was to determine the effectiveness of upper-surface leading-edge blowing in producing increased lift and lift-drag ratios for an HSCT-class airplane at takeoff, initial climb, and approach to landing. The research was conducted by modifying an existing model of a generic HSCT configuration. The model comprised a cranked delta wing with an inboard sweep of 71°, an outboard sweep of 50°, and a relatively thin airfoil. Because the leading edge was thin, the blowing slot, unlike conventional leading-edge blowing tangent to the leading edge, was behind the leading edge and blowing aft tangent to the upper surface. Furthermore, because of fabrication constraints, the blowing slot was located only on the inboard two-thirds of the wing 71°-sweep leading edge.

The results indicate that this blowing technique had little beneficial effect on increasing lift coefficient C_L and lift-drag ratio L/D and often had detrimental effects. The technique did affect the upper-surface flow field. The major thrust-induced effects were a small stabilizing rotation of the pitching-moment curve, a slight increase in L/D_{max} for the cruise wing at low blowing rates, and a decrease of L/D_{max} for the high-lift wing configuration with the Krueger flap at high blowing rates. The major thrust-included effects were a greater stabilizing rotation and downward translation of the pitching-moment curve and significant losses in L/D_{eq} with increasing blowing rates. In general this blowing method, *at the test conditions,* did not provide the benefits that had been predicted. In previous studies, blowing at the leading edge and other locations on the wing surface has often shown favorable lift and drag increments. This and other studies have shown that not all such concepts are successful. *However, this investigation covered a limited parameter space and does not attest to the effectiveness possible with other geometries and conditions.*

NASA Langley Research Center
Hampton, VA 23681-0001
March 7, 1996

References

1. Campbell, Bryan A.; Applin, Zachary T.; Kemmerly, Guy T.; Coe, Paul L., Jr.; Owens, D. Bruce; Gile, Brenda E.; Parikh, Pradip G.; and Smith, Don: *Subsonic Investigation of a Leading-Edge Boundary Layer Control Suction System on a High-Speed Civil Transport Configuration.* NASA/TM-1999-209700, 1999.

2. Campbell, Bryan A.; Applin, Zachary T.; and Kemmerly, Guy T.: *Subsonic Aerodynamic Assessment of Vortex Flow Management Devices on High-Speed Civil Transport Configuration.* NASA/TP-1999-209693, 1999.

3. Greenwell, D. I.; and Wood, N. J.: Control of Asymmetric Vortical Flows. AIAA-91-3272, Sept. 1991.

4. Bean, D. E.; Greenwell, D. I.; and Wood, N. J.: Vortex Control Technique for the Attenuation of Fin Buffet. *J. Aircr.*, vol. 30, no. 6, Nov.–Dec. 1993, pp. 847–853.

5. Craig, K.: Computational Study of Blowing on Delta Wings at High Alpha. *J. Aircr.*, vol. 30, no. 6, Nov.–Dec. 1993, pp. 833–839.

6. Wood, N. J.; and Roberts, L.: Control of Vortical Lift on Delta Wings by Tangential Leading Edge Blowing. AIAA-87-0158, Jan. 1987.

7. Gentry, Garl L., Jr.; Quinto, P. Frank; Gatlin, Gregory M.; and Applin, Zachary T.: *The Langley 14- by 22-Foot Subsonic Tunnel—Description, Flow Characteristics, and Guide for Users*. NASA TP-3008, 1990.

8. Rae, William H., Jr.; and Pope, Alan: *Low-Speed Tunnel Testing*. John Wiley & Sons, Inc., 1984.

9. Herriot, John G.: *Blockage Corrections for Three-Dimensional-Flow Closed-Throat Wind Tunnels, With Consideration of the Effect of Compressibility*. NACA Rep. 995, 1950. (Supersedes NACA RM A7B28.)

10. Engler, R. J.; and Williams, R. M.: Test Techniques for High Lift, Two-Dimensional Airfoils With Boundary Layer and Circulation Control For Application to Rotary Wing Aircraft. *Canadian Aeronaut. & Space J.*, vol. 19, no. 3, Mar. 1973, pp. 95–108.

11. Engler, R. J.: *Two-Dimensional Subsonic Wind Tunnel Investigations of a Cambered 30-Percent Thick Circulation Control Airfoil*. Naval Ship Research and Development Center Technical Note, TN-AL-201, May 1972. (Also available from DTIC as AD 913 411L.)

Table I. Geometric Characteristics of Basic Model

[Wing reference area is defined by extending wing inboard leading edge and outboard trailing edge of cruise configuration planform projection to centerline. (See fig. 2(b).)]

Aspect ratio	2.116
Reference area, ft^2	10.664
Gross area, ft^2	11.005
Span, ft	4.750
Root chord, ft	5.288
Tip chord, ft	0.529
Reference $\bar{c}$, ft	3.071
Leading-edge sweep, inboard, deg	71.0
Leading-edge sweep, outboard, deg	50.0

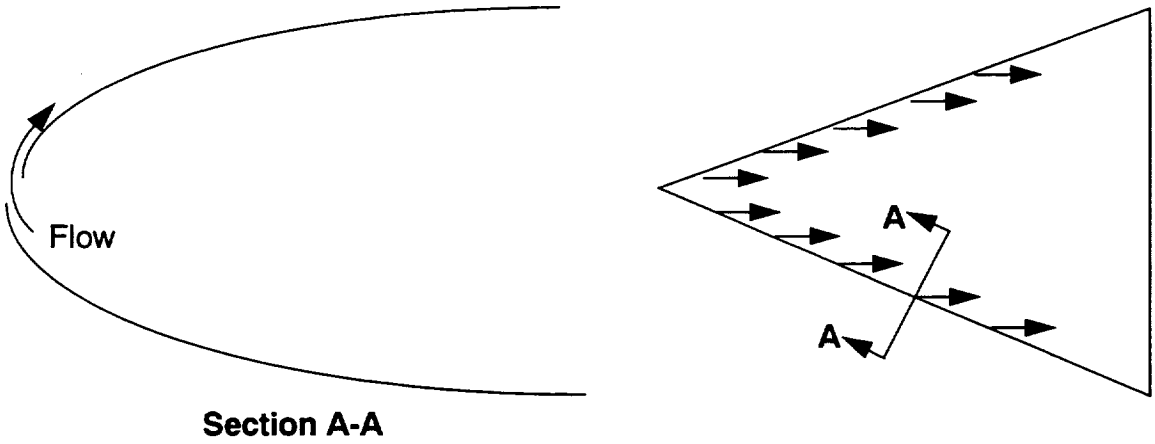

(a) Conventional leading-edge blowing.

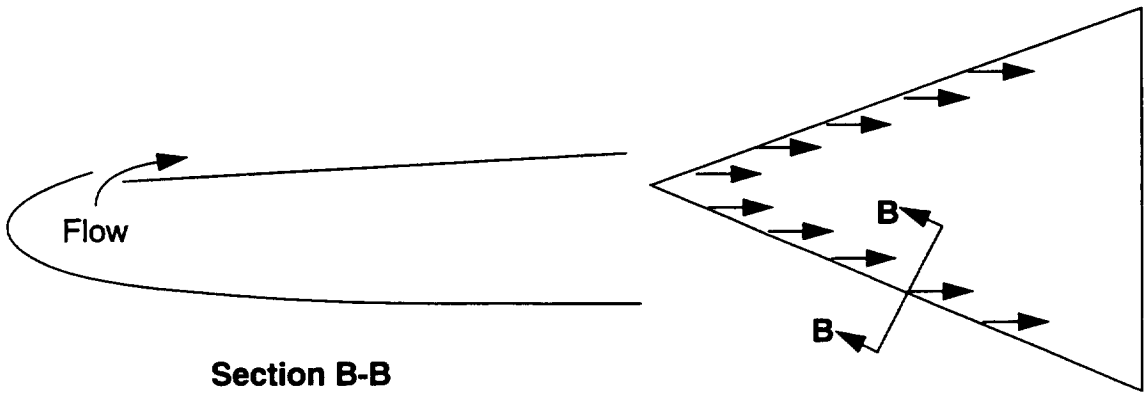

(b) Upper-surface leading-edge blowing.

Figure 1. Conventional leading-edge blowing and test model upper-surface leading-edge blowing.

L-94-03220

(a) Model in Langley 14- by 22-Foot Subsonic Tunnel.

Figure 2. 71/50 generic high-speed model.

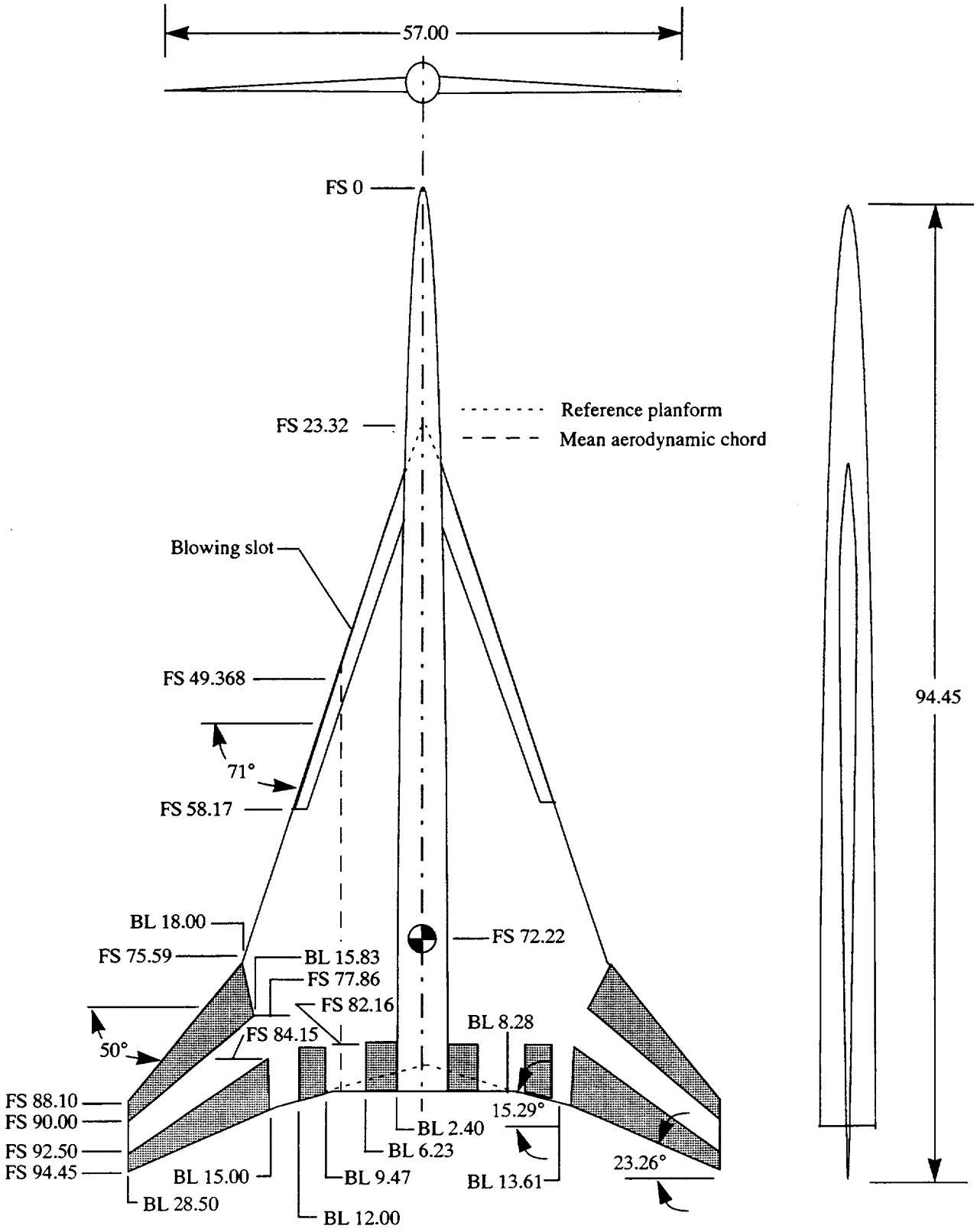

(b) Model geometry. All linear dimensions are in inches.

Figure 2. Continued.

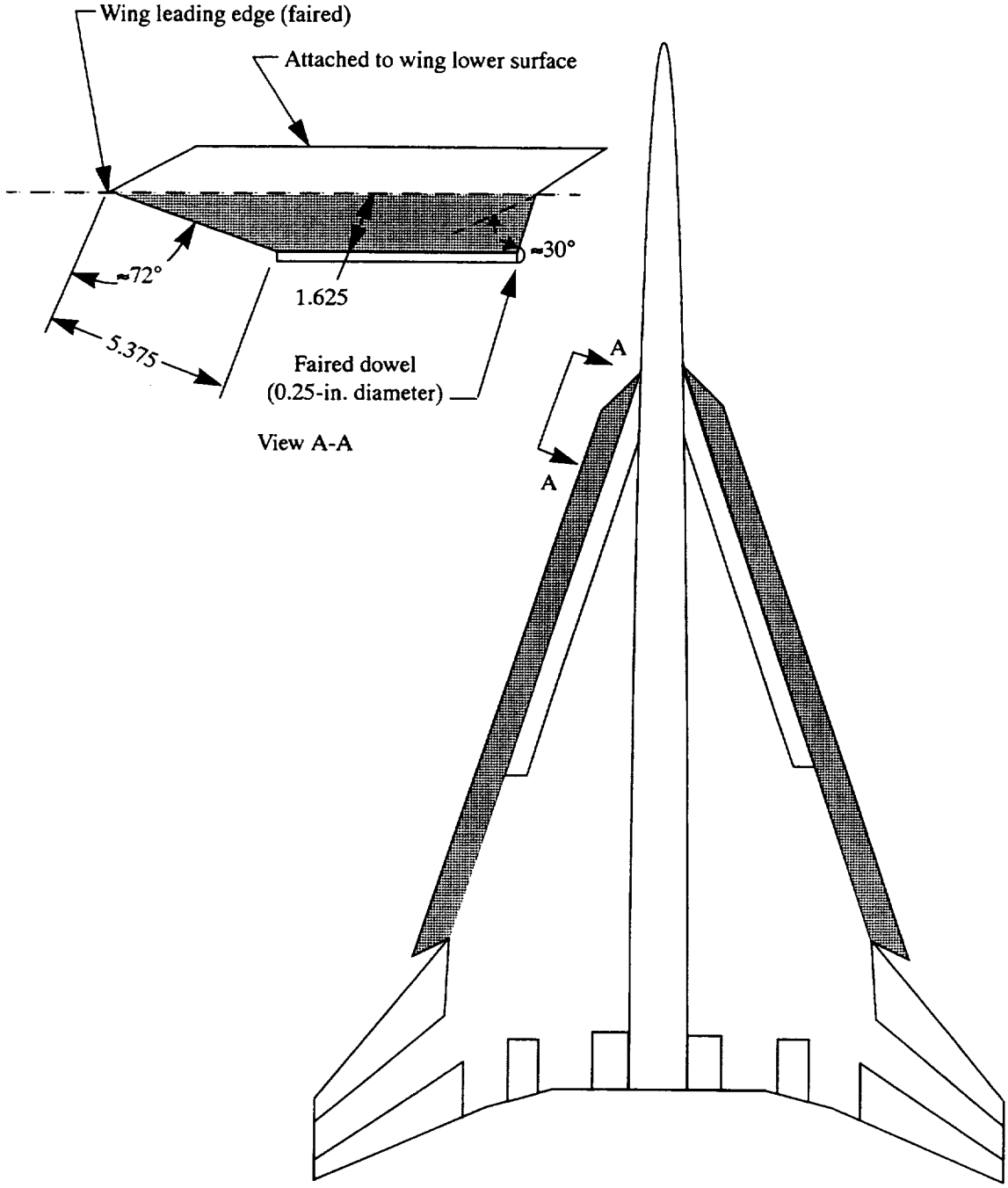

(c) Krueger flap geometry. All linear dimensions are in inches.

Figure 2. Continued.

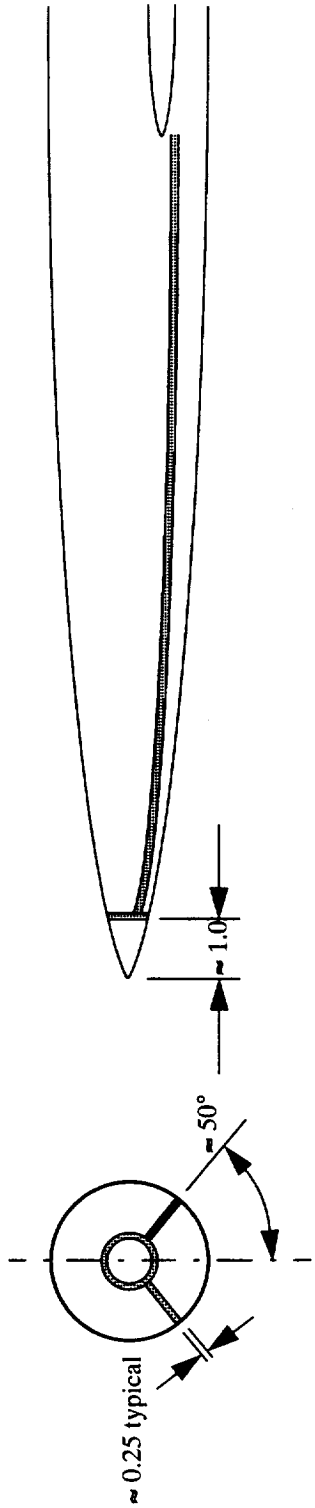

(d) Forebody test grit pattern. All linear dimensions are in inches.

Figure 2. Concluded.

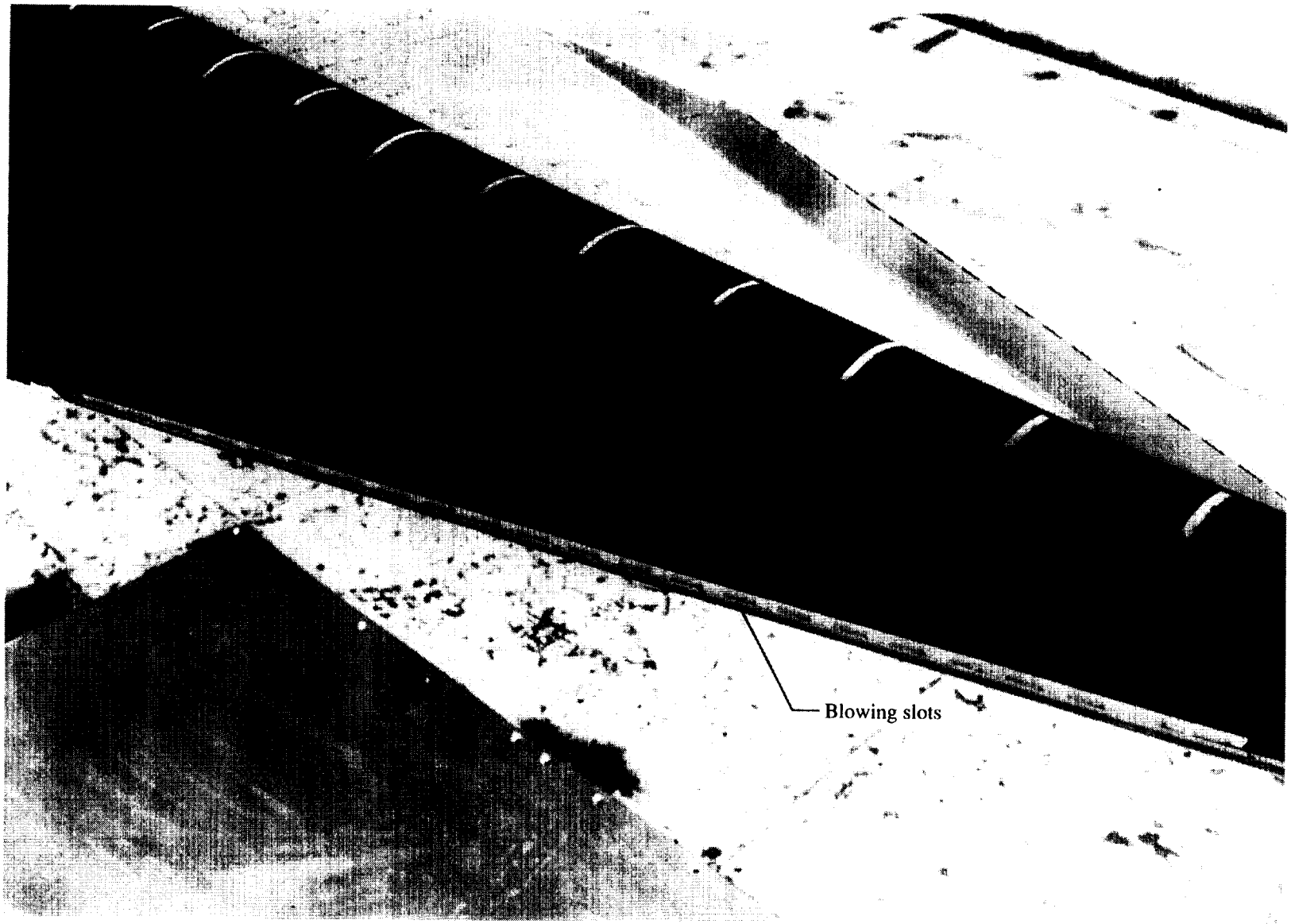

L-94-03219

(a) Close-up of leading-edge blowing slots.

Figure 3. Details of 71/50 model wing leading-edge blowing system.

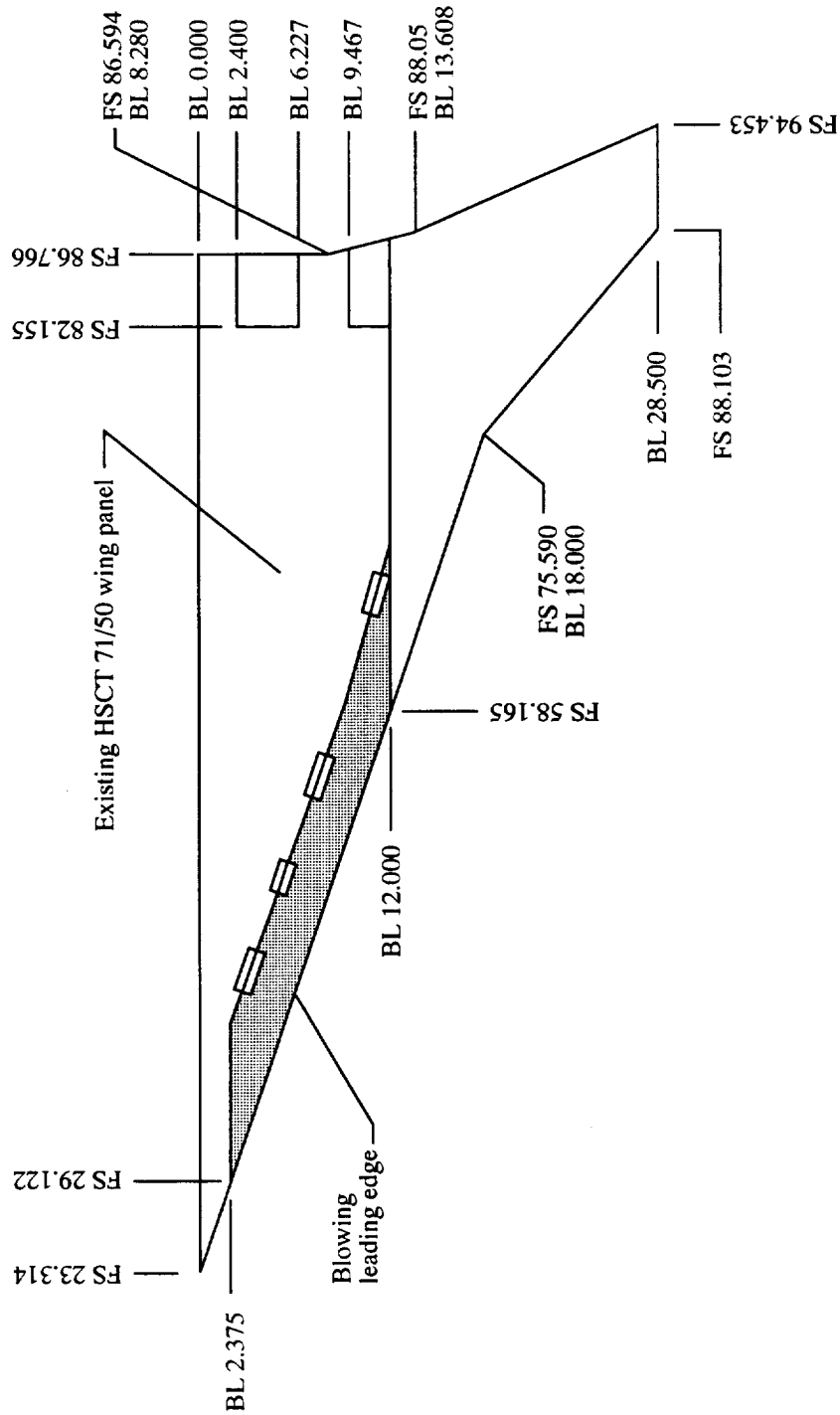

(b) Wing assembly plan view (left side shown). All linear dimensions are in inches.

Figure 3. Continued.

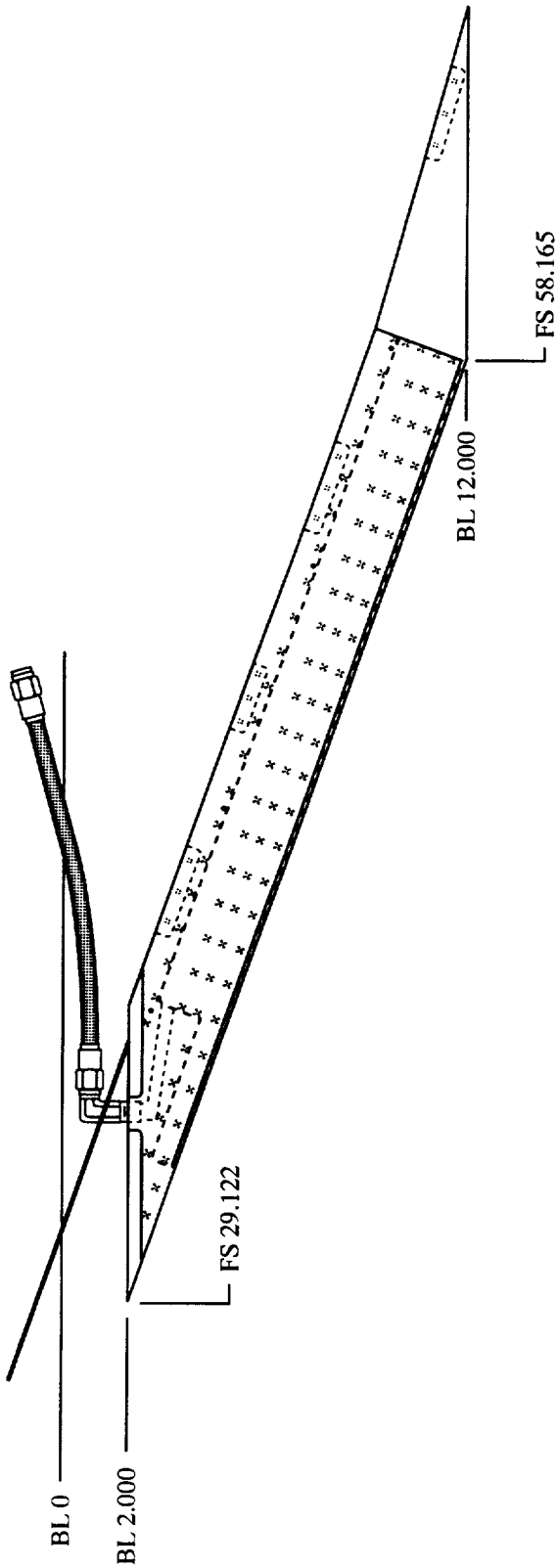

(c) Leading-edge detail (left side shown). All dimensions are in inches.

Figure 3. Continued.

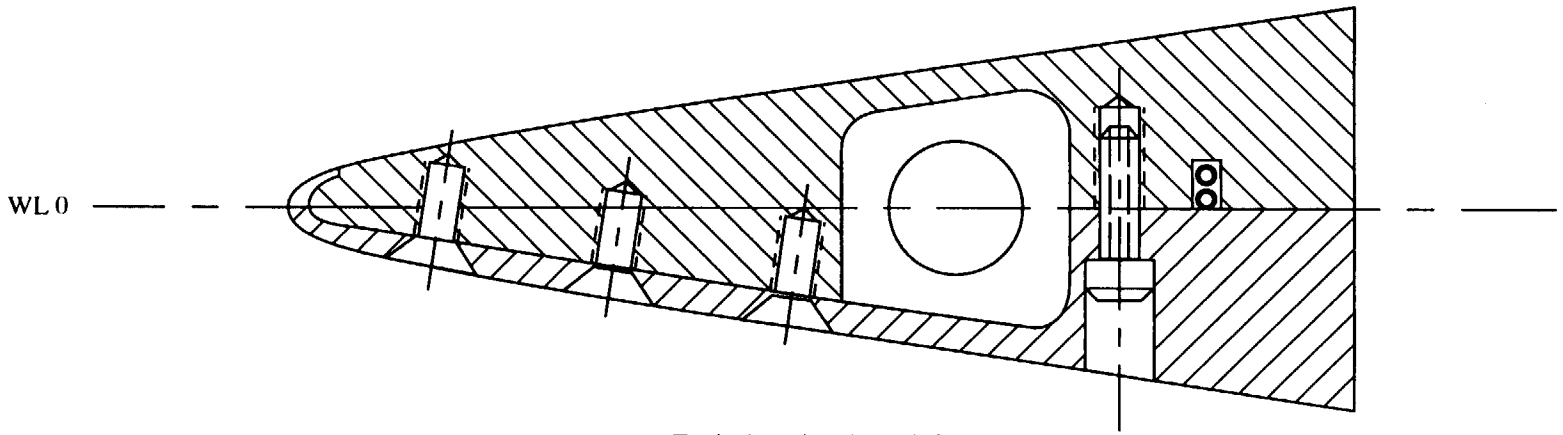

Typical section through fences

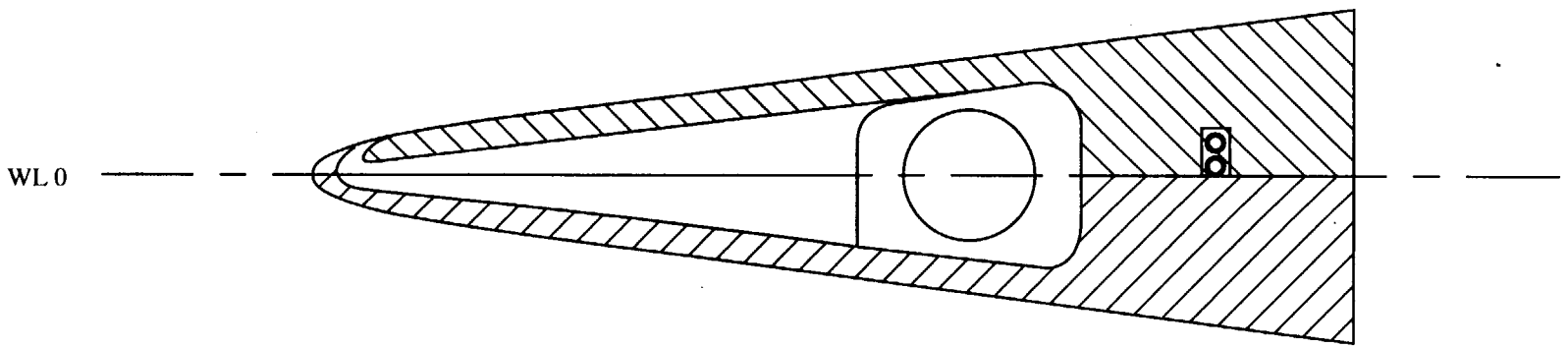

Typical section through air passage

(d) Typical cross sections of leading edge (left side shown).

Figure 3. Continued.

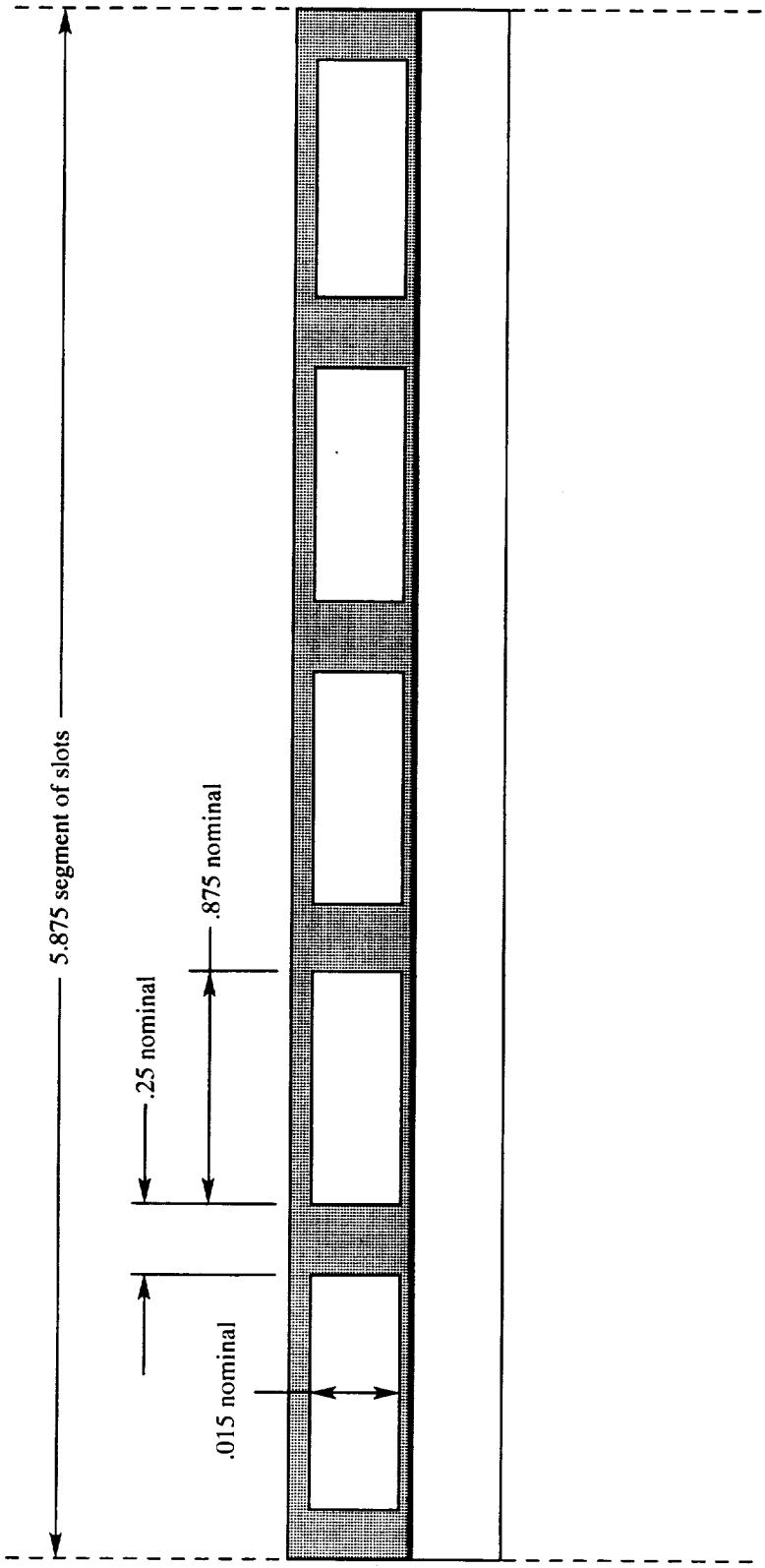

(e) Typical cross section of blowing slot. All linear dimensions are in inches (not to scale).

Figure 3. Concluded.

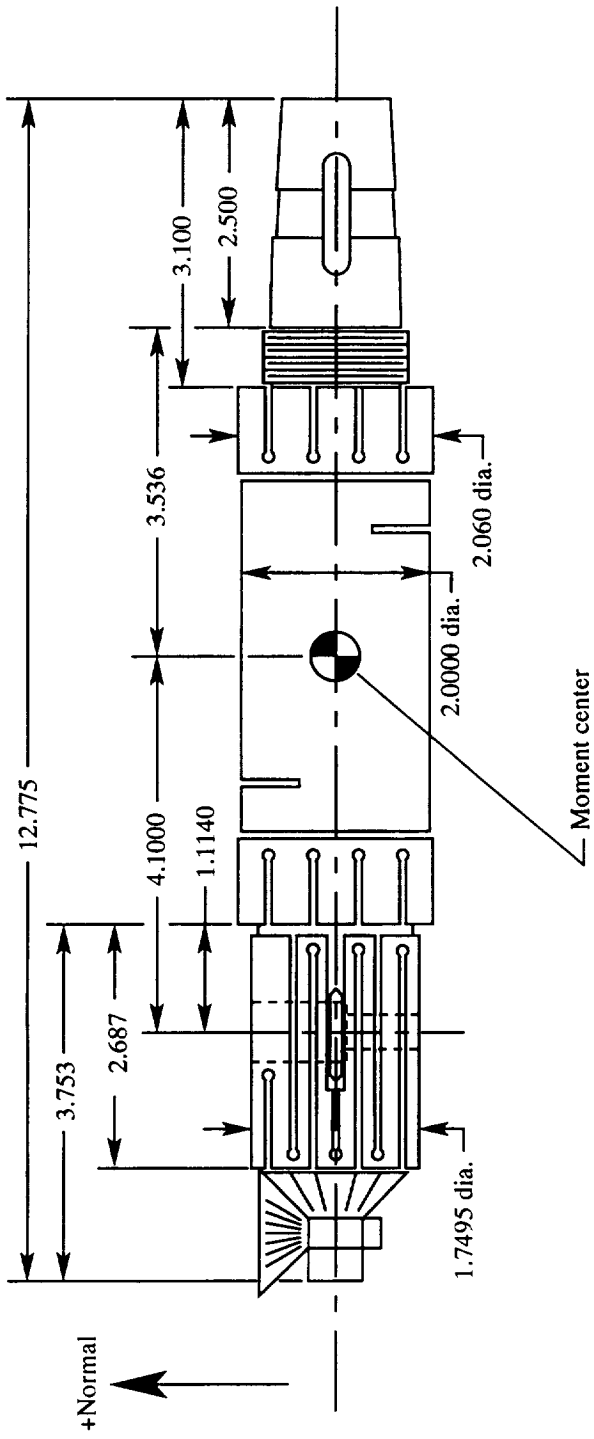

Figure 4. Langley VST-3 strain-gage balance. All linear dimensions are in inches (not to scale).

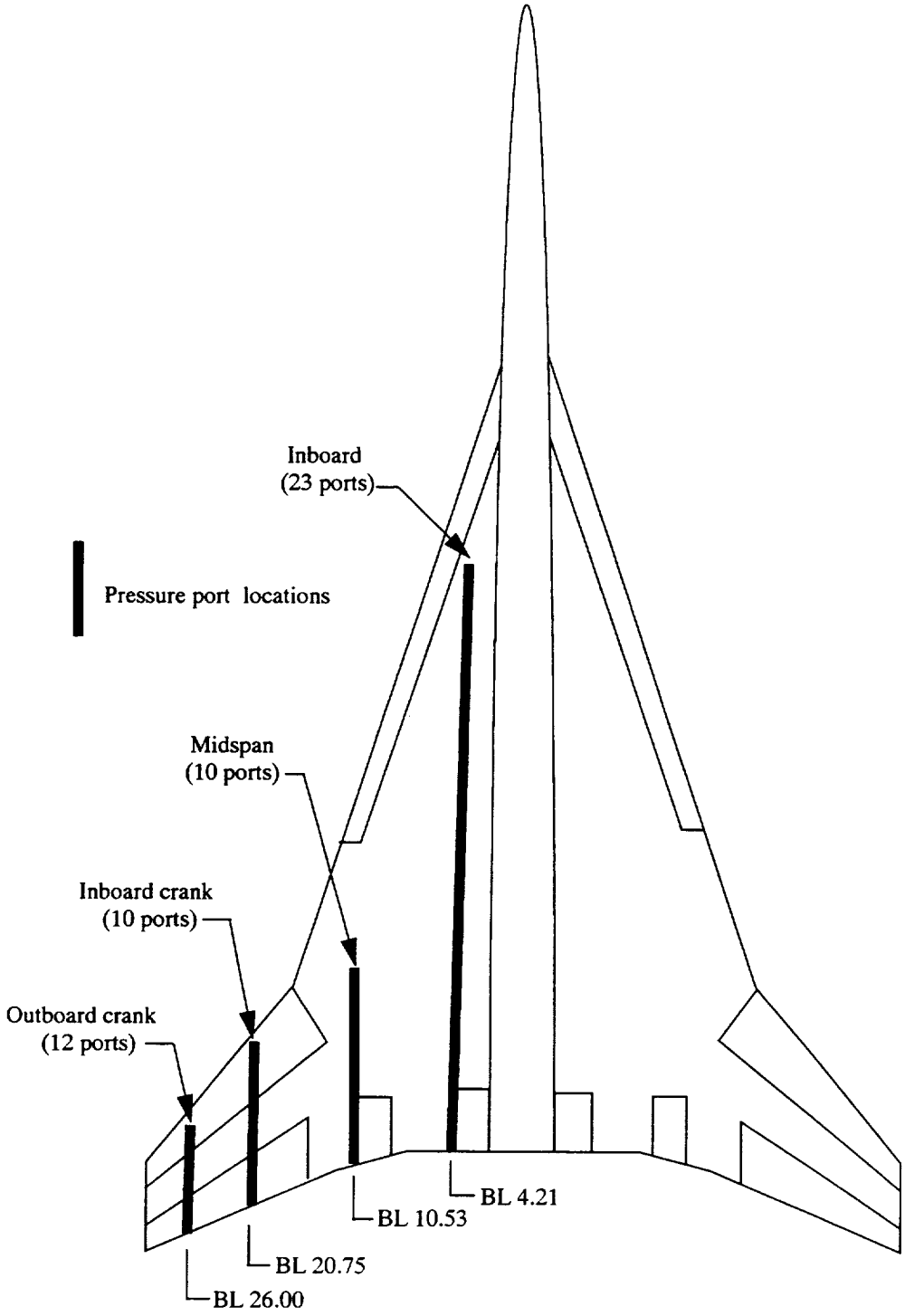

Figure 5. Pressure port locations on 71/50 model.

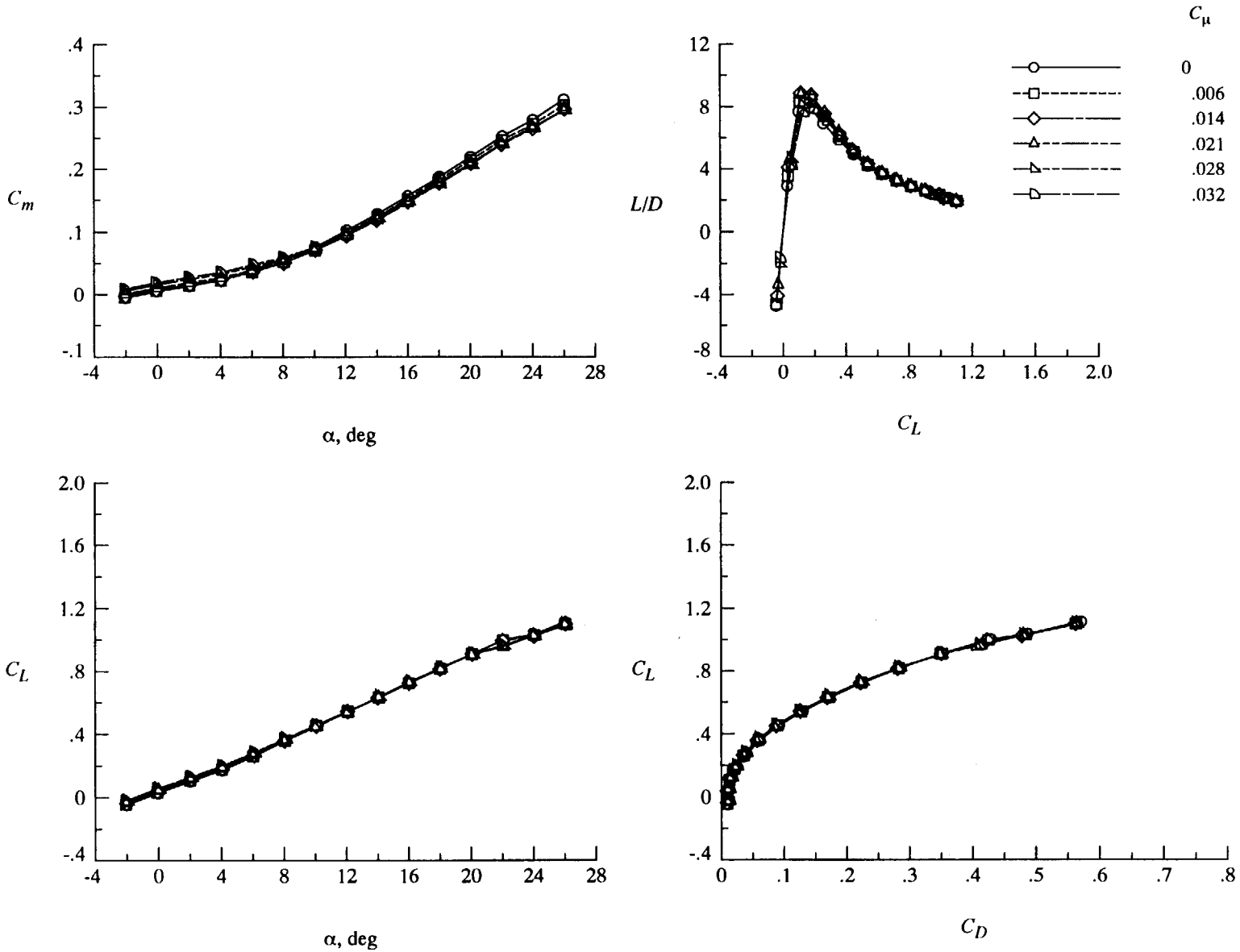

Figure 6. Effect of blowing coefficient on longitudinal aerodynamics of cruise wing. Thrust removed and q_∞ = 70 psf.

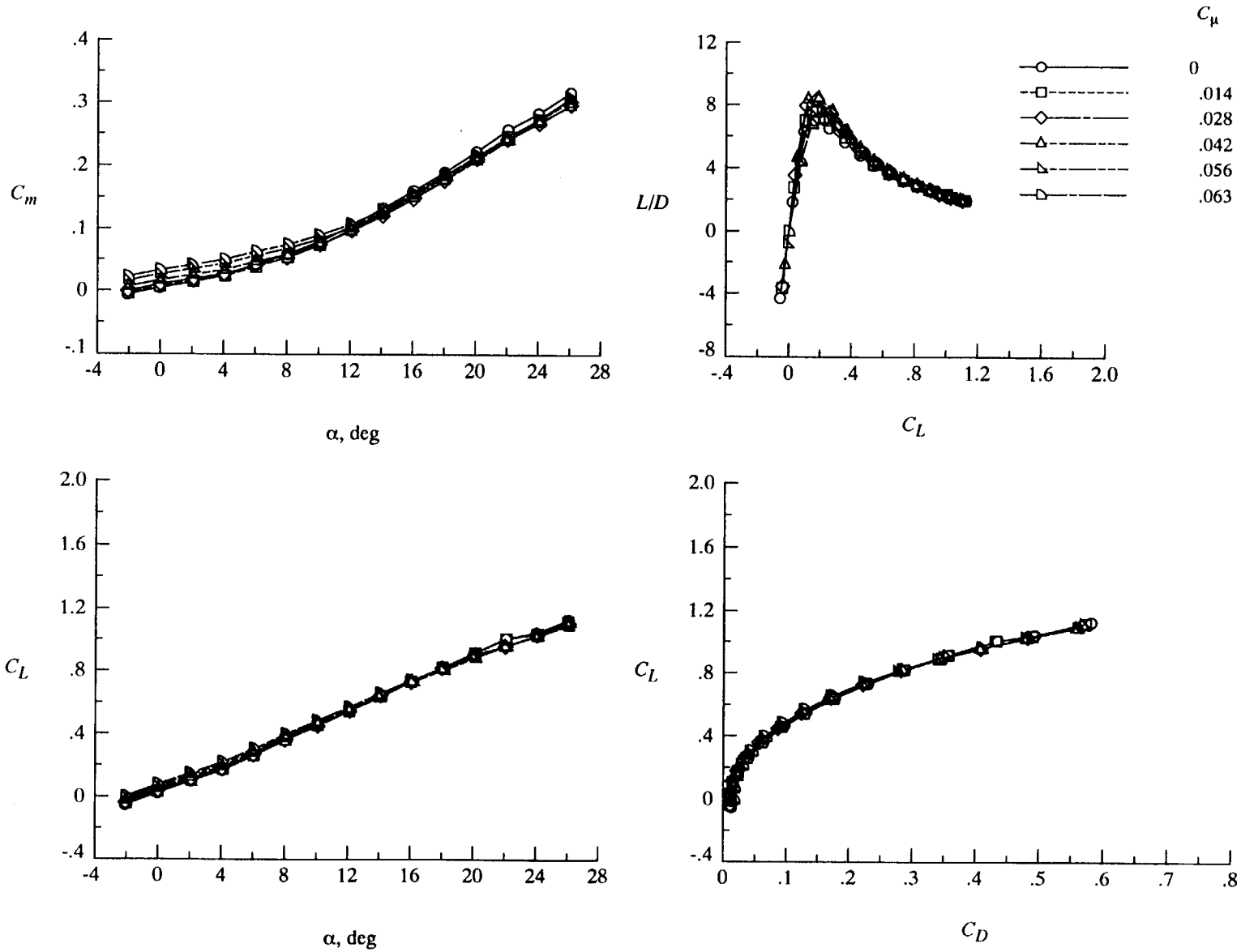

Figure 7. Effect of blowing coefficient on longitudinal aerodynamics of cruise wing. Thrust removed and q_∞ = 35 psf.

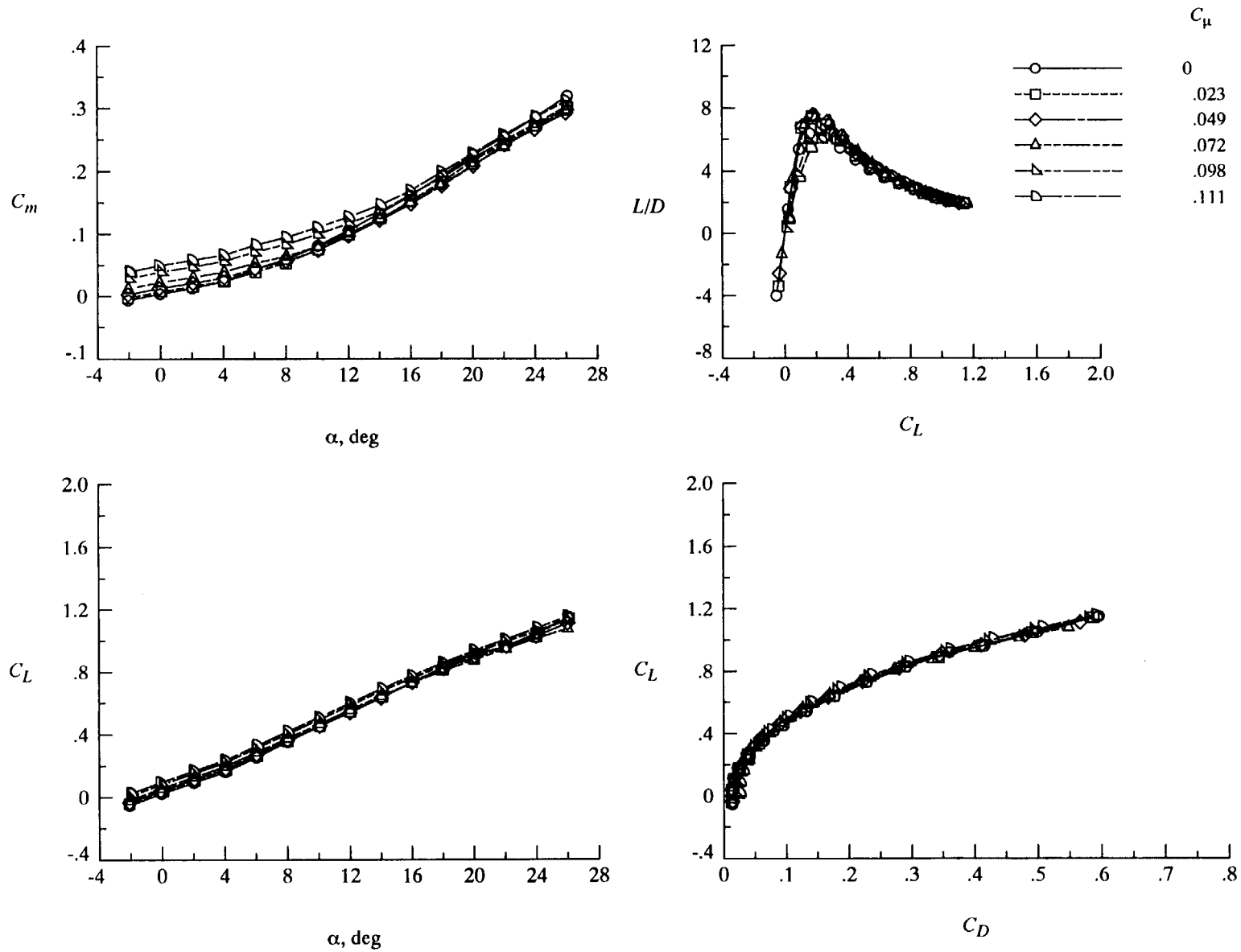

Figure 8. Effect of blowing coefficient on longitudinal aerodynamics of cruise wing. Thrust removed and q_∞ = 20 psf.

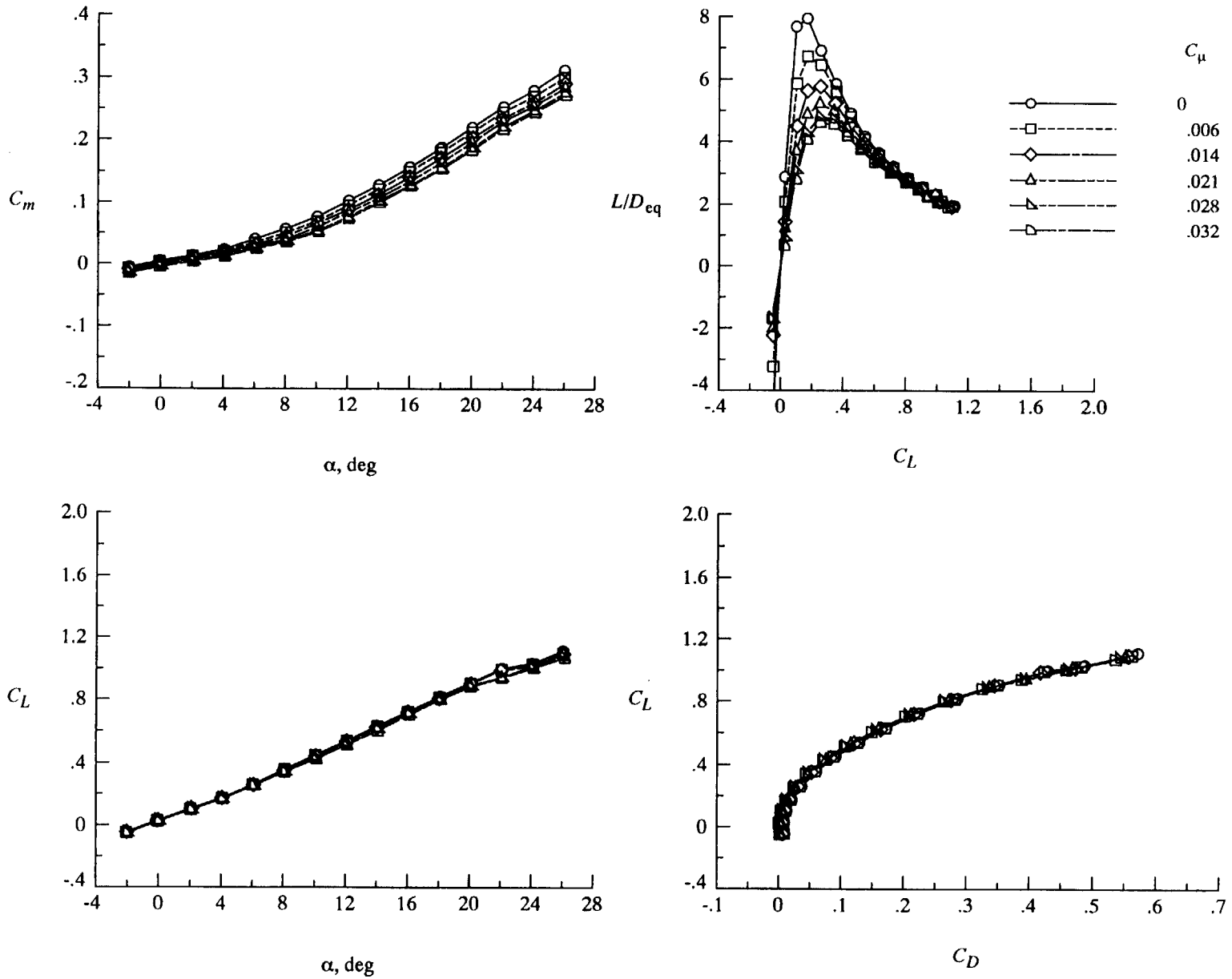

Figure 9. Effect of blowing coefficient on longitudinal aerodynamics of cruise wing. Thrust included and q_∞ = 70 psf.

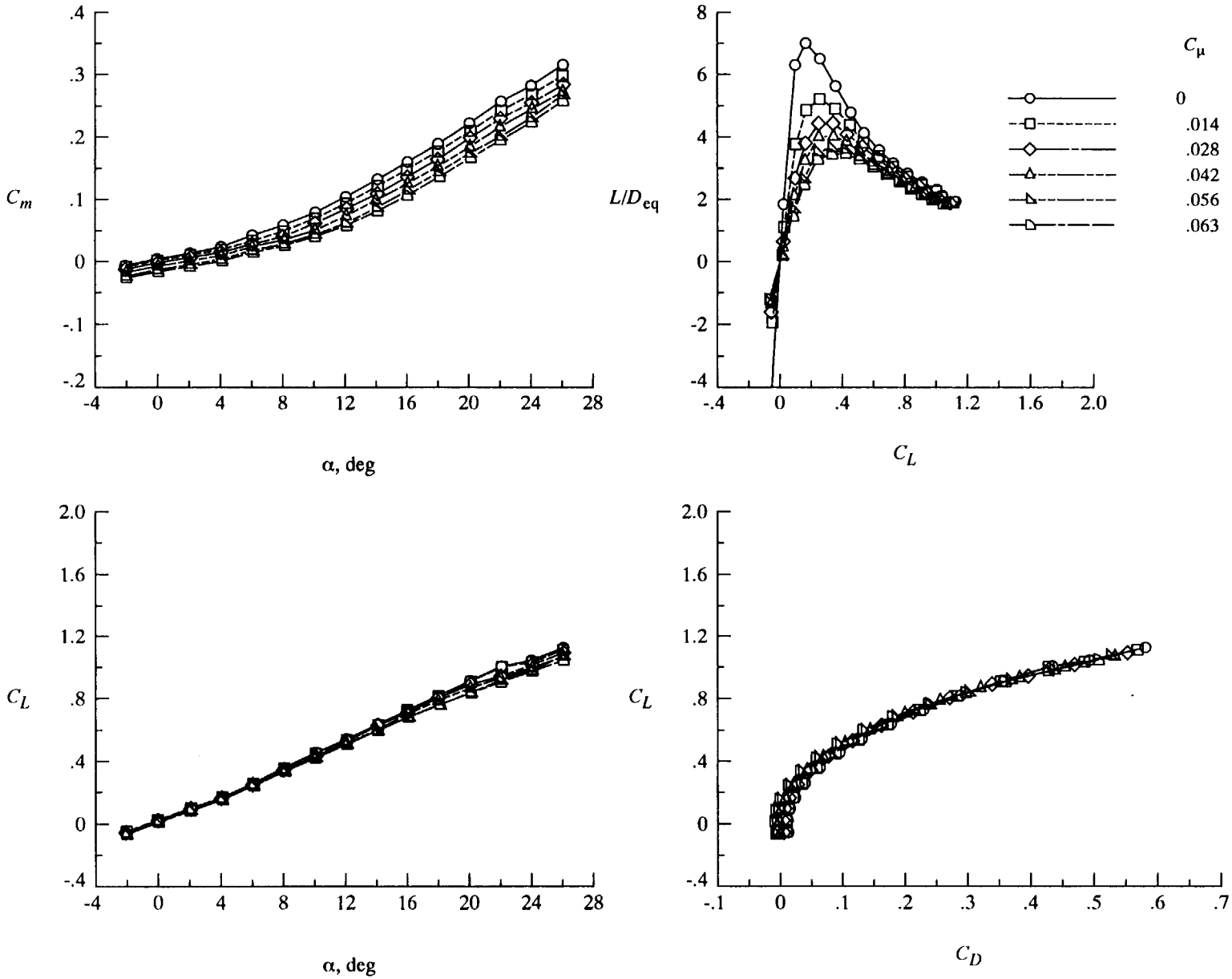

Figure 10. Effect of blowing coefficient on longitudinal aerodynamics of cruise wing. Thrust included and q_∞ = 35 psf.

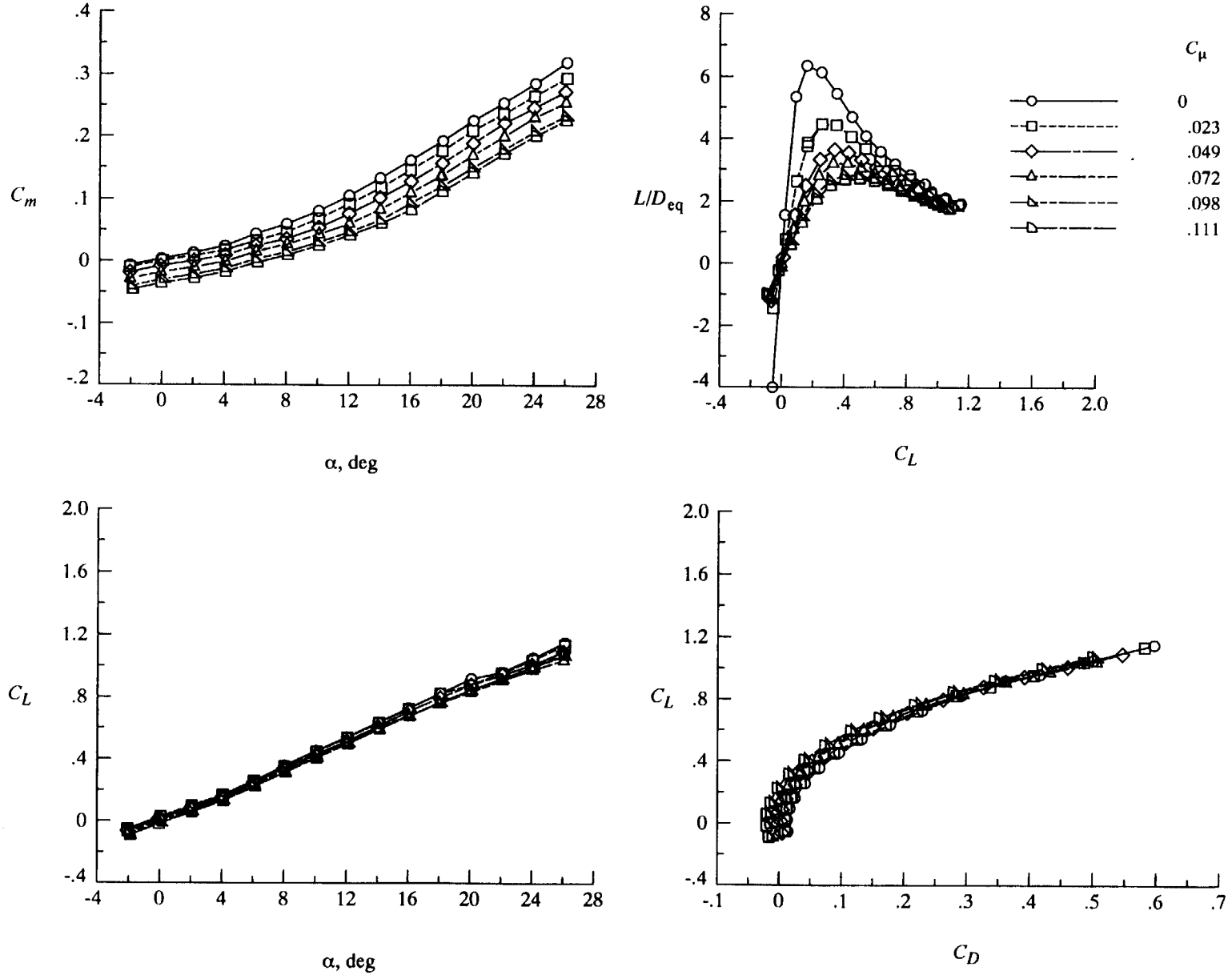

Figure 11. Effect of blowing coefficient on longitudinal aerodynamics of cruise wing. Thrust included and q_∞ = 20 psf.

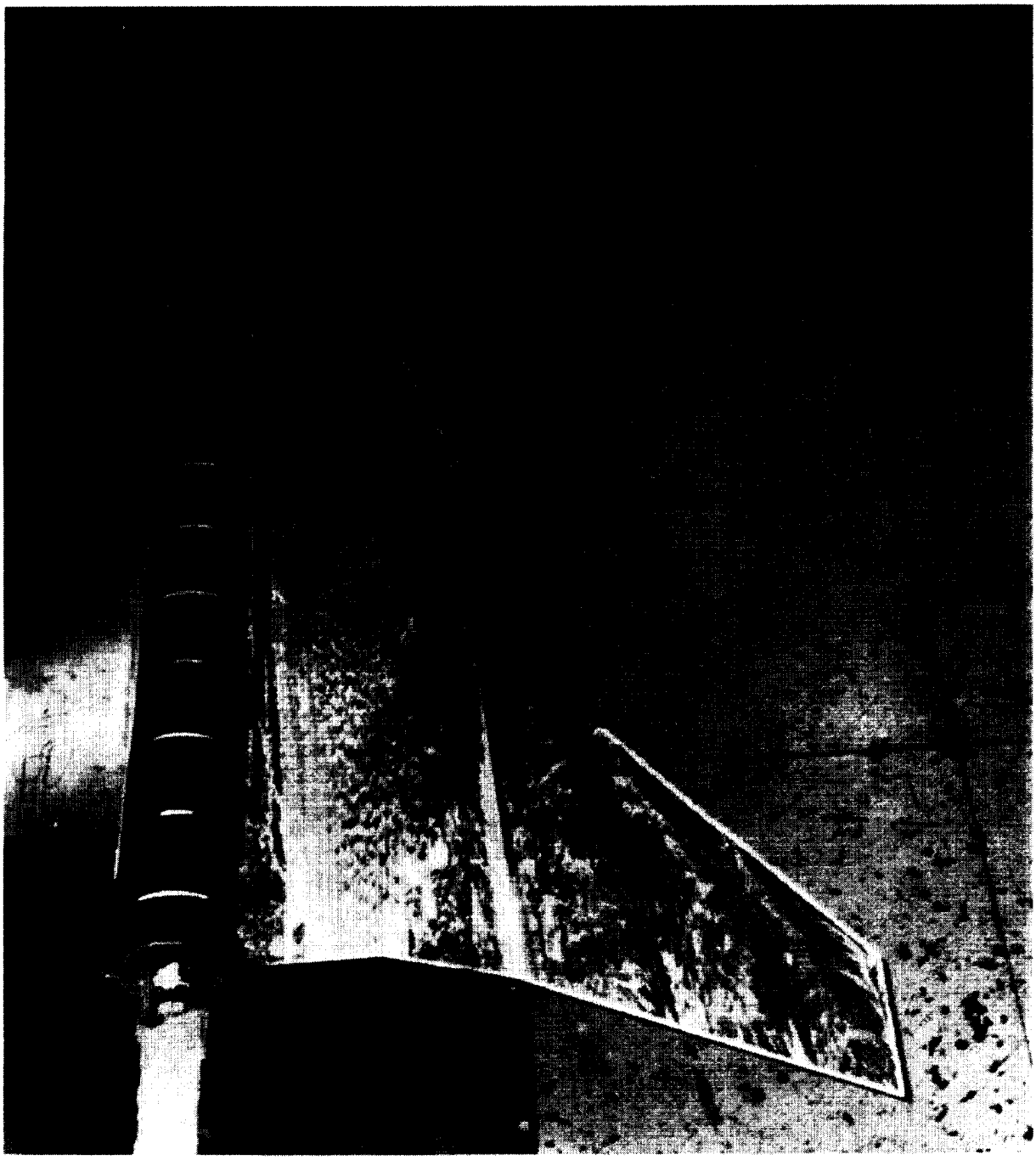

Figure 12. Surface flow visualization of cruise wing. $\alpha = 4°$; $C_\mu = 0$; and $q_\infty = 20$ psf.

Figure 13. Surface flow visualization of cruise wing. $\alpha = 4°$; $C_\mu = 0.050$; and $q_\infty = 20$ psf.

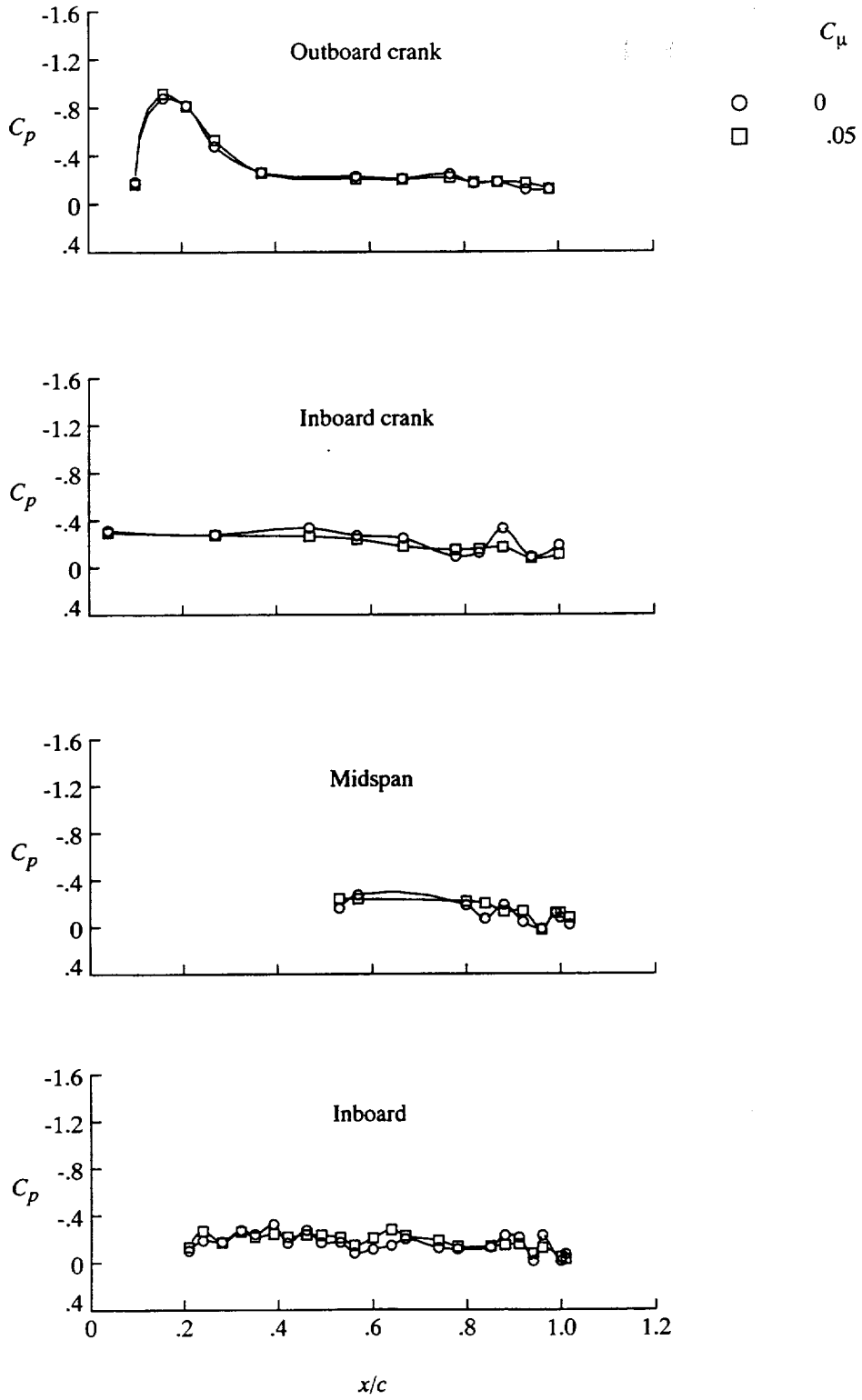

Figure 14. Effect of blowing coefficient on surface pressure distributions of cruise wing. $\alpha = 4°$ and $q_\infty = 20$ psf.

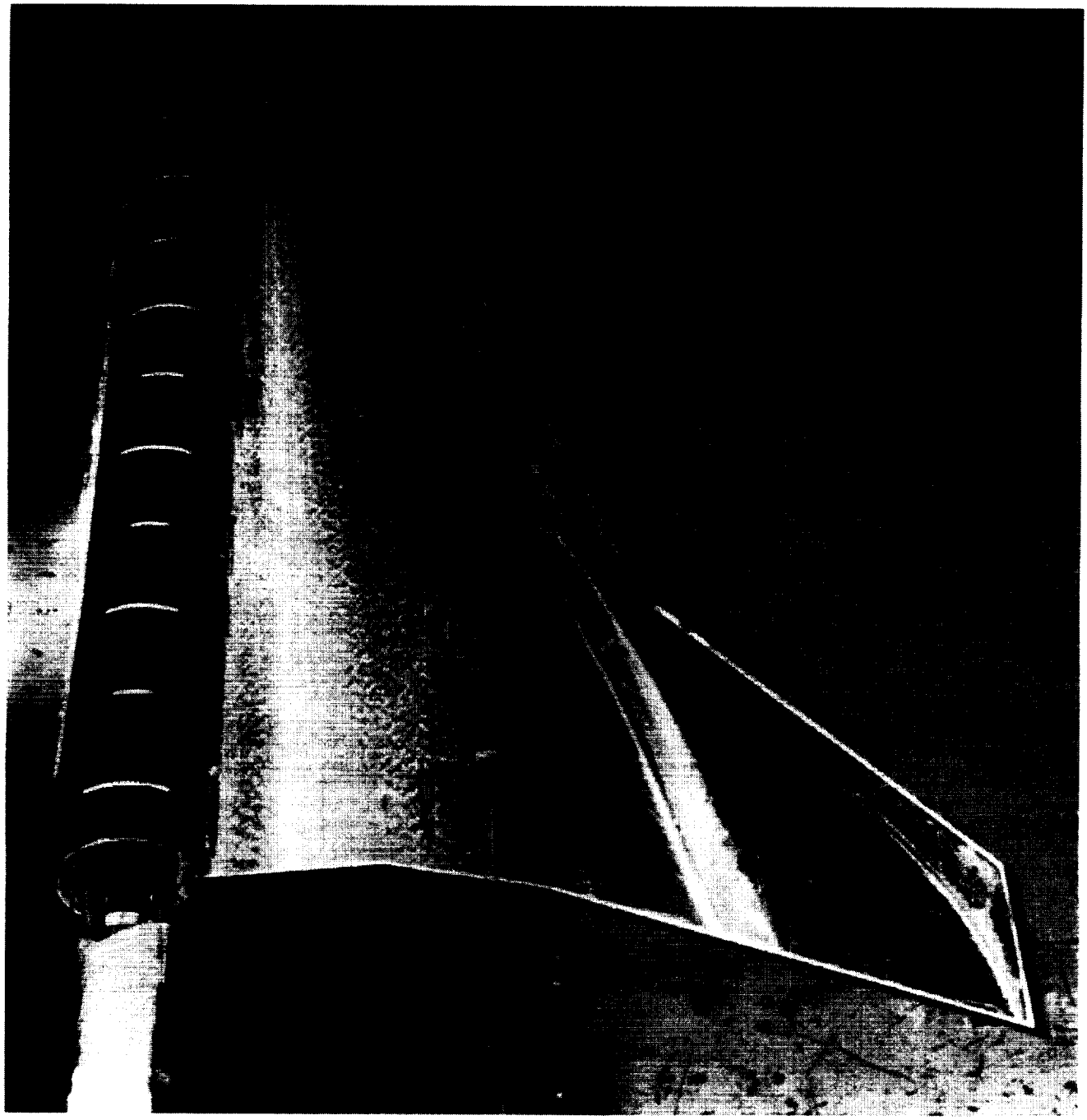

Figure 15. Surface flow visualization of cruise wing. $\alpha = 10°$; $C_\mu = 0$; and $q_\infty = 20$ psf.

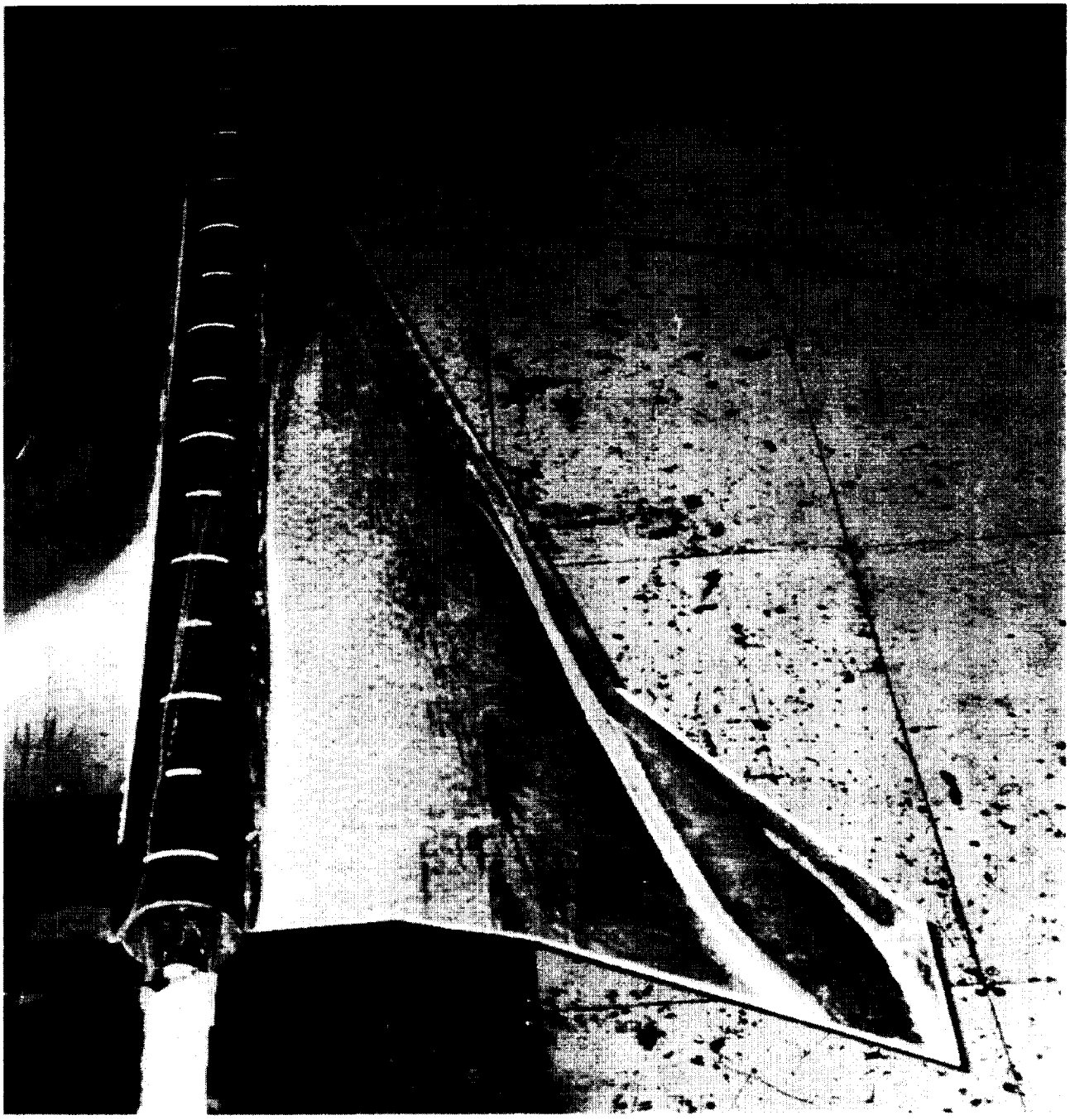

Figure 16. Surface flow visualization of cruise wing. $\alpha = 10°$; $C_\mu = 0.023$; and $q_\infty = 20$ psf.

Figure 17. Surface flow visualization of cruise wing. $\alpha = 10°$; $C_\mu = 0.050$; and $q_\infty = 20$ psf.

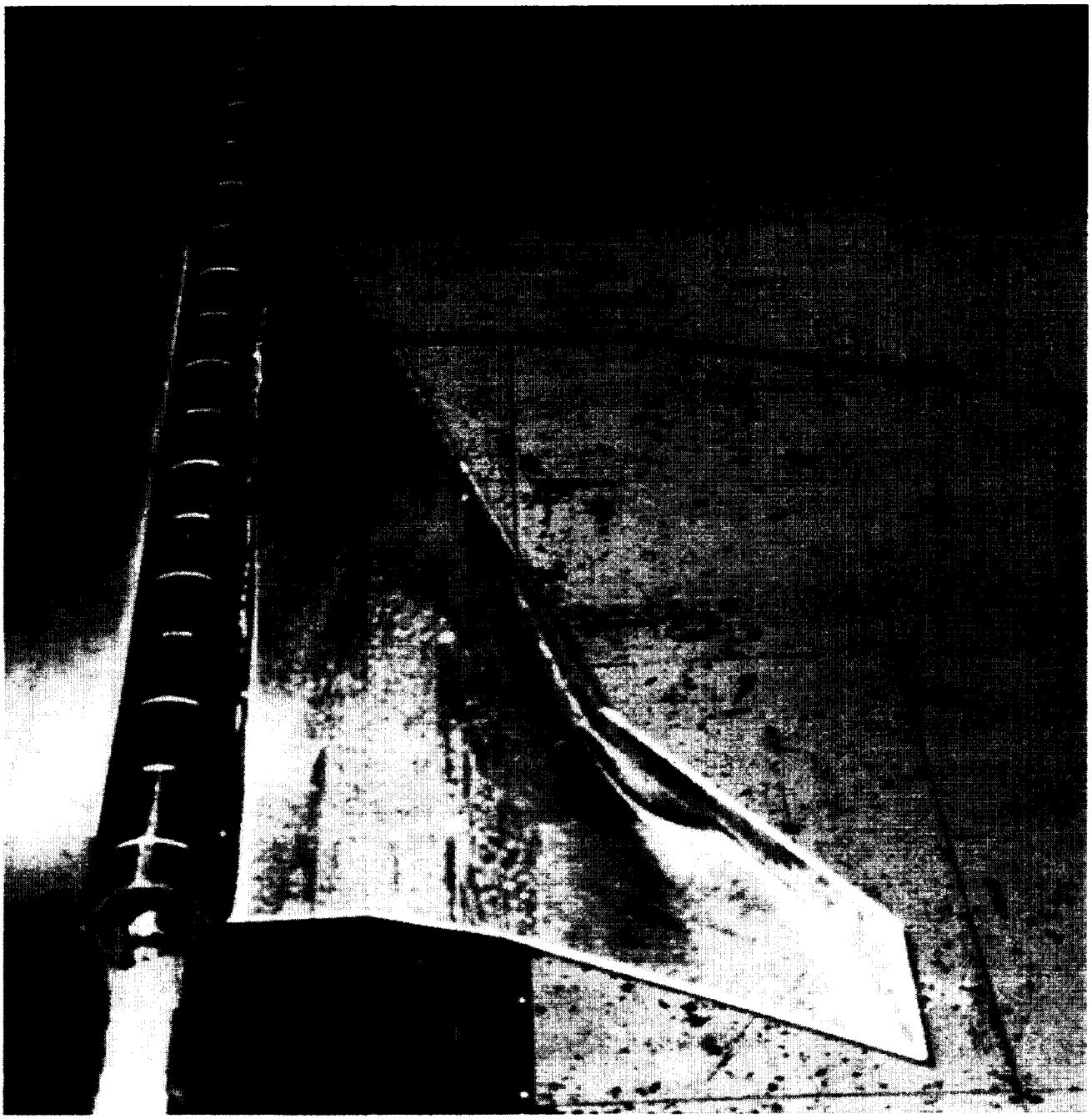

Figure 18. Surface flow visualization of cruise wing. $\alpha = 10°$; $C_\mu = 0.072$; and $q_\infty = 20$ psf.

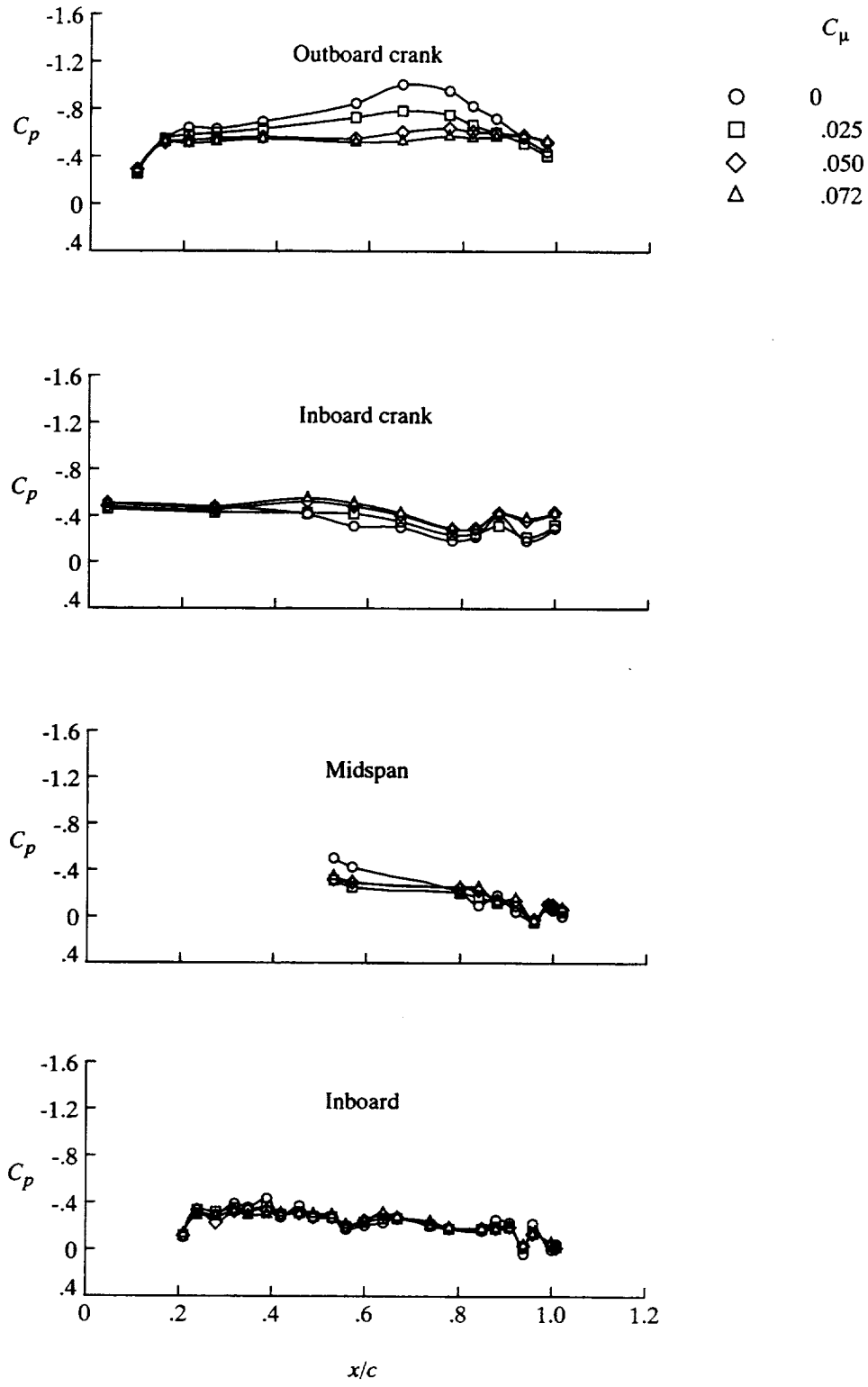

Figure 19. Effect of blowing coefficient on surface pressure distributions of cruise wing. α = 10° and q_∞ = 20 psf.

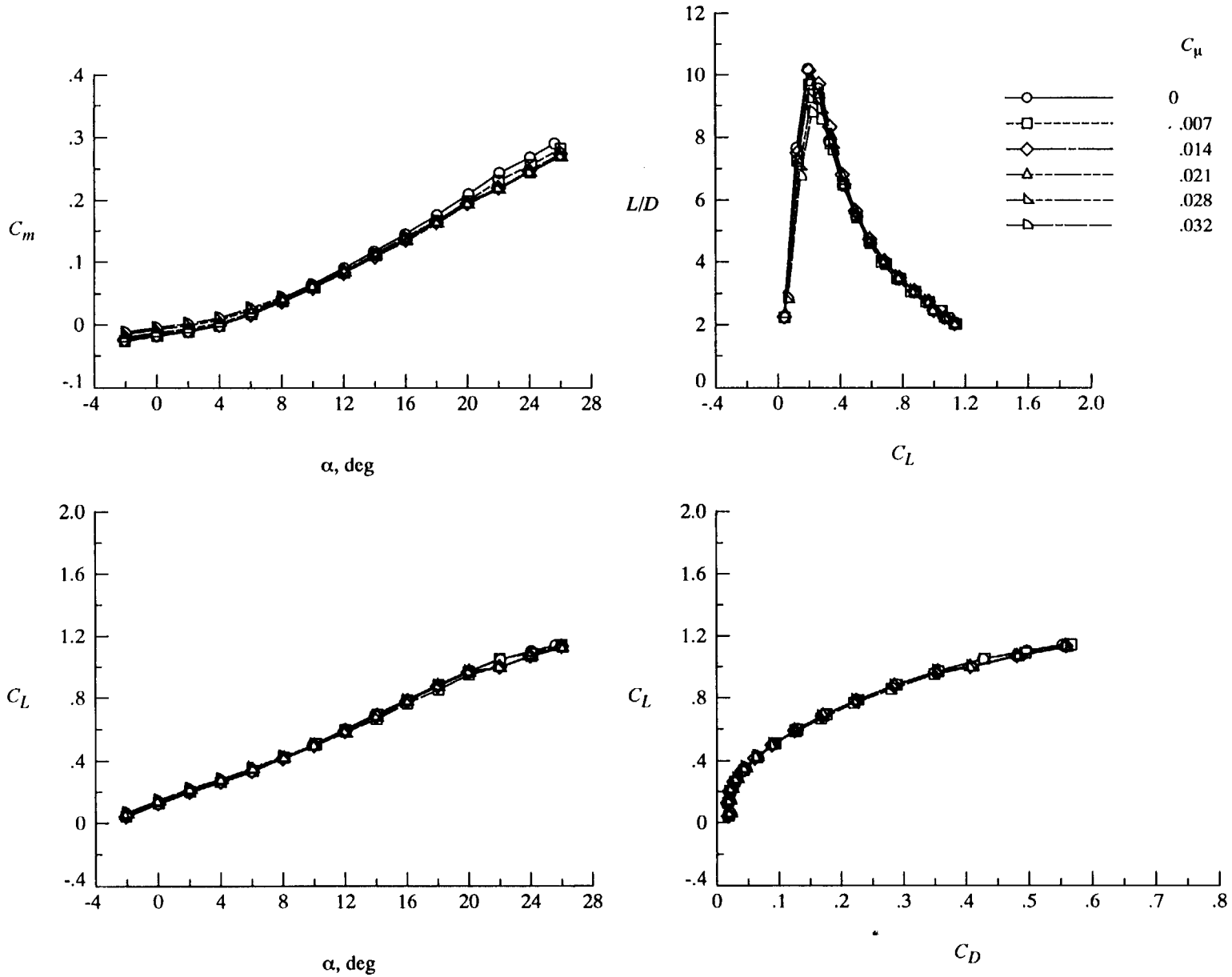

Figure 20. Effect of blowing coefficient on longitudinal aerodynamics of high-lift wing. Thrust removed and q_∞ = 70 psf.

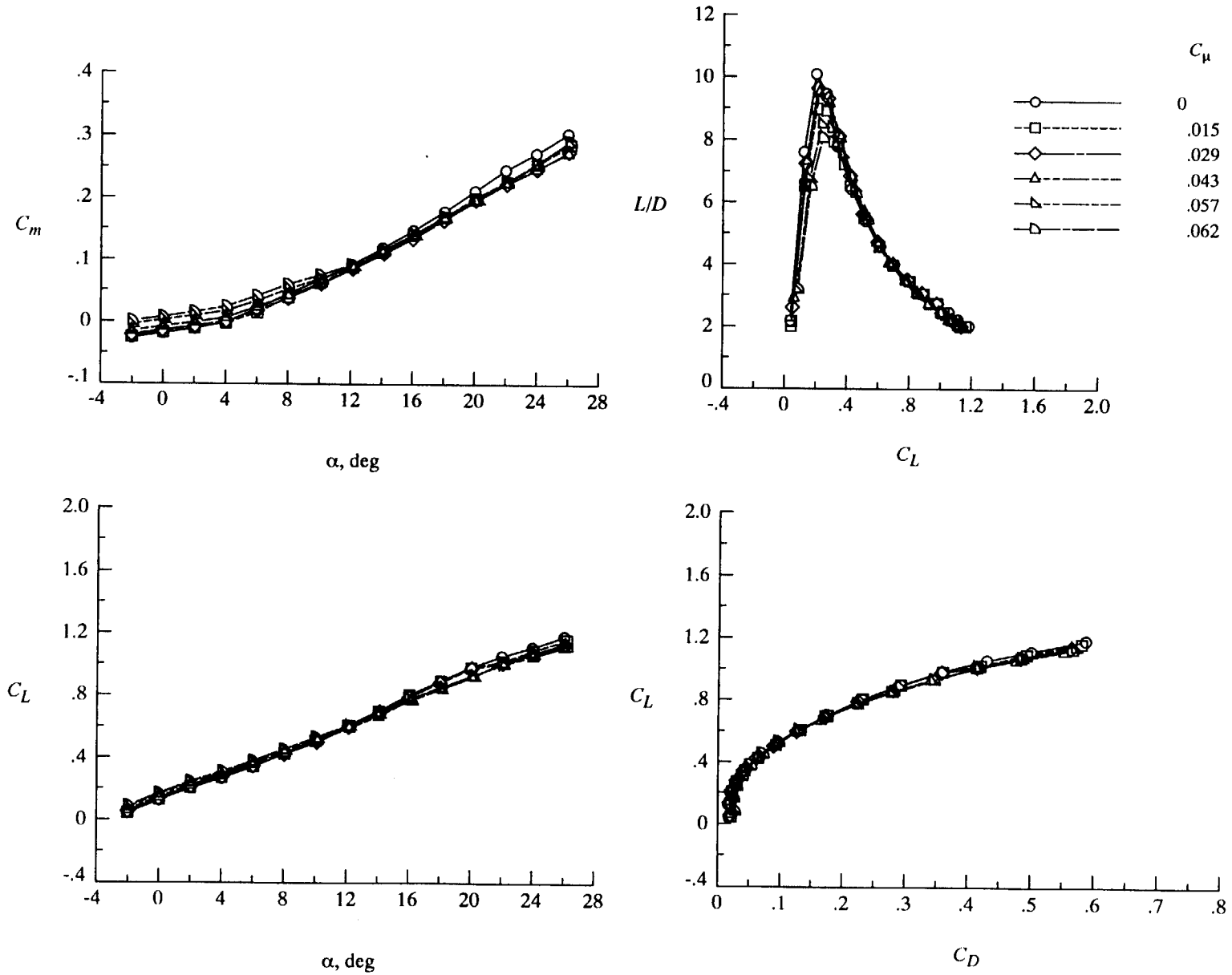

Figure 21. Effect of blowing coefficient on longitudinal aerodynamics of high-lift wing. Thrust removed and q_∞ = 35 psf.

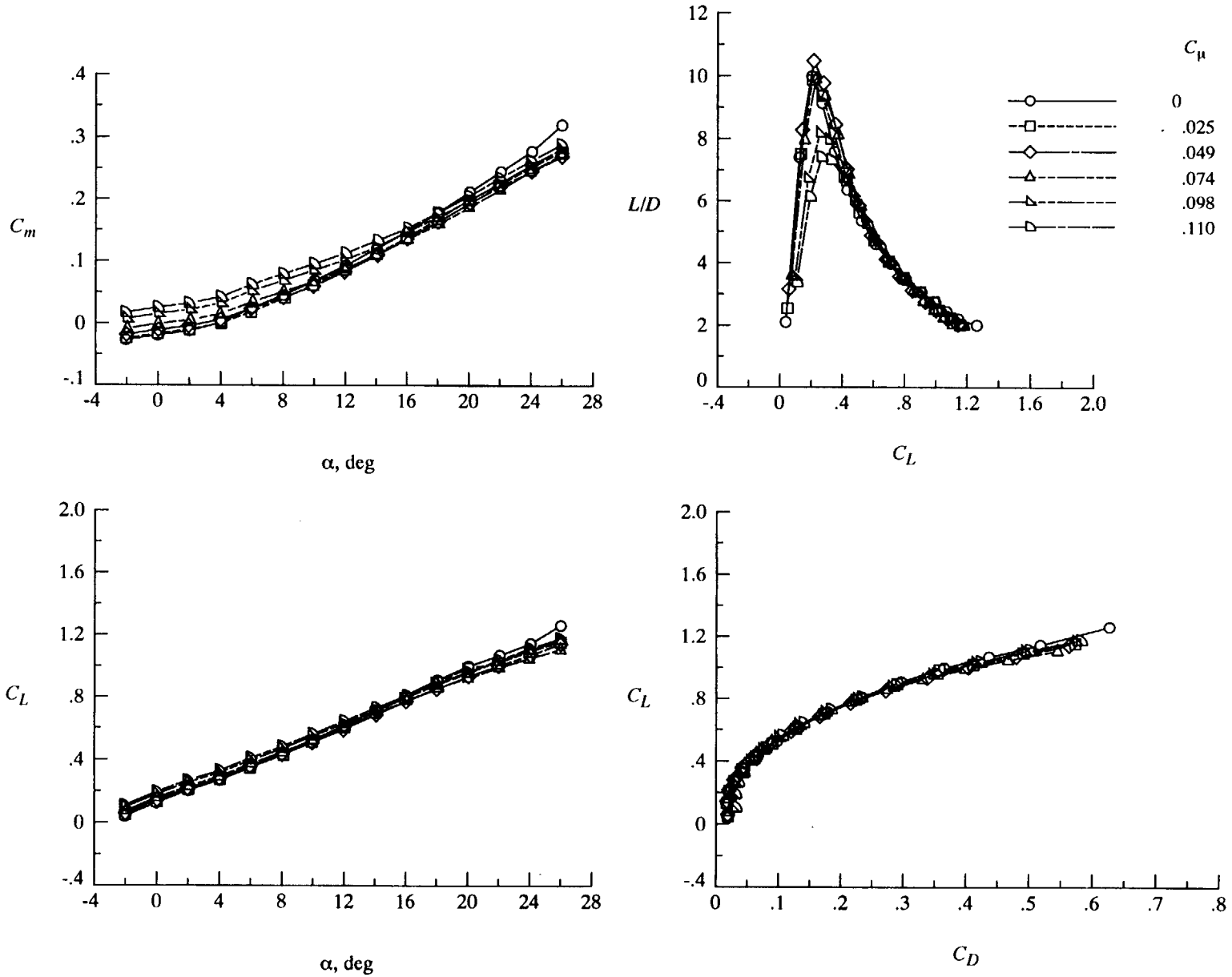

Figure 22. Effect of blowing coefficient on longitudinal aerodynamics of high-lift wing. Thrust removed and q_∞ = 20 psf.

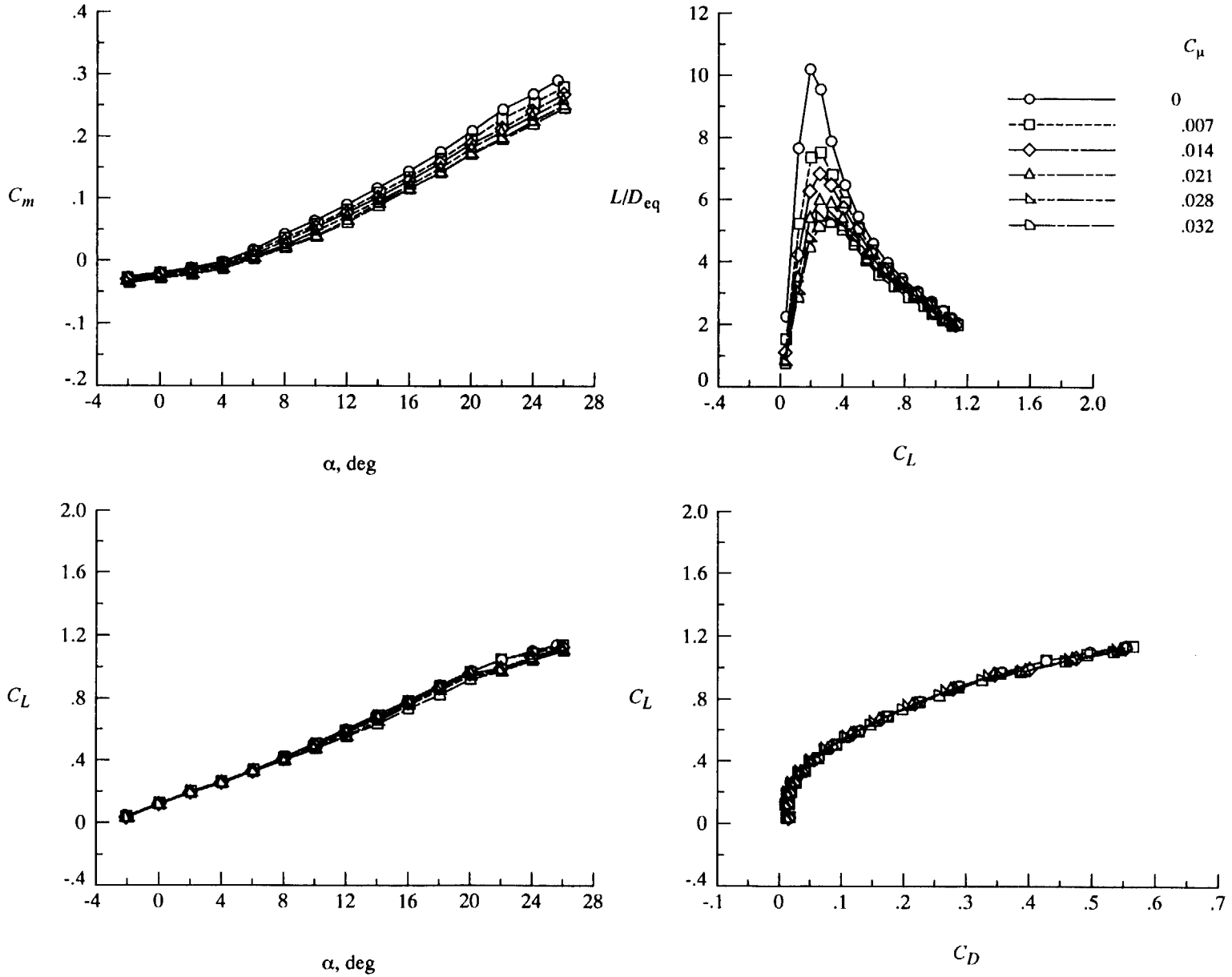

Figure 23. Effect of blowing coefficient on longitudinal aerodynamics of high-lift wing. Thrust included and q_∞ = 70 psf.

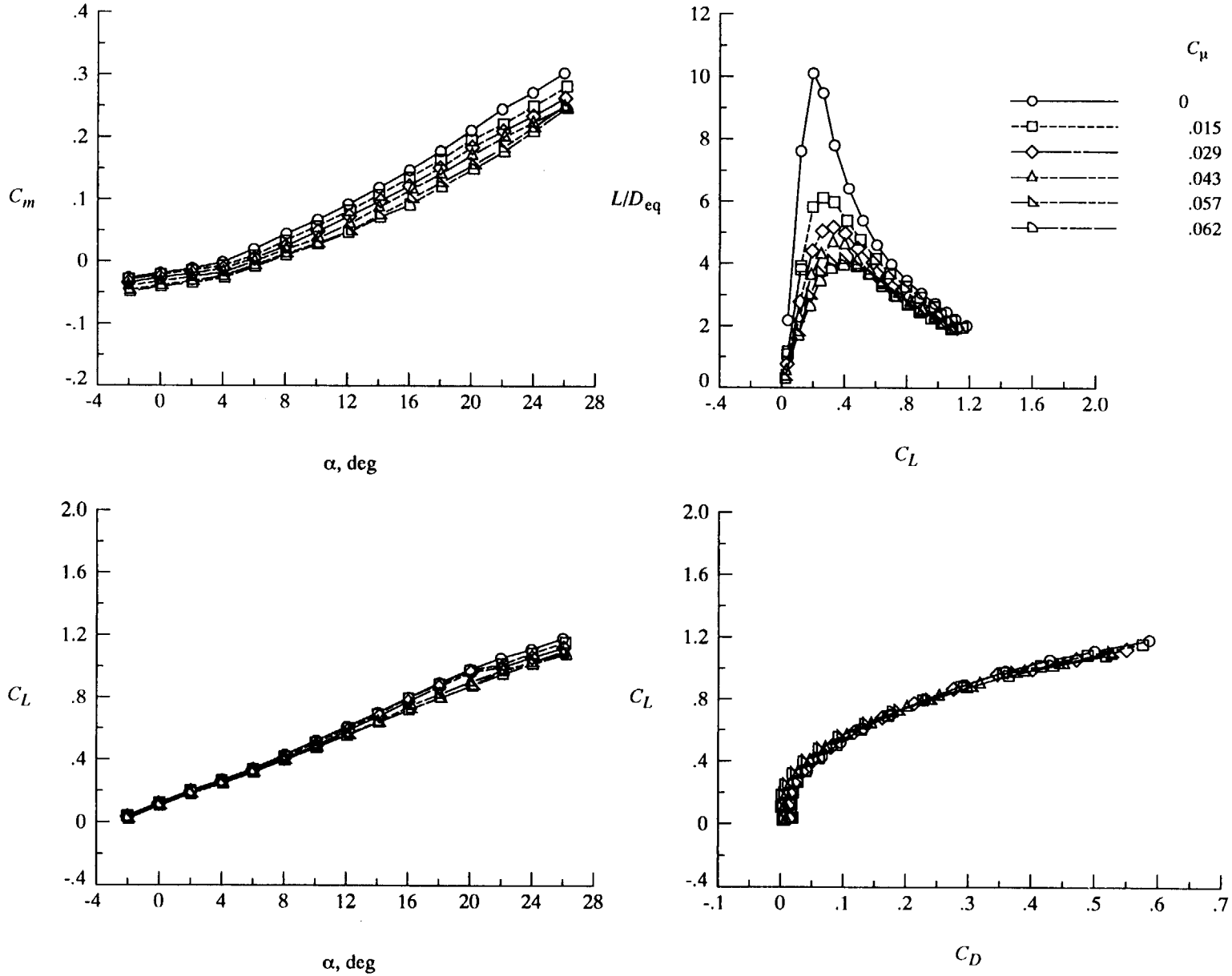

Figure 24. Effect of blowing coefficient on longitudinal aerodynamics of high-lift wing. Thrust included and q_∞ = 35 psf.

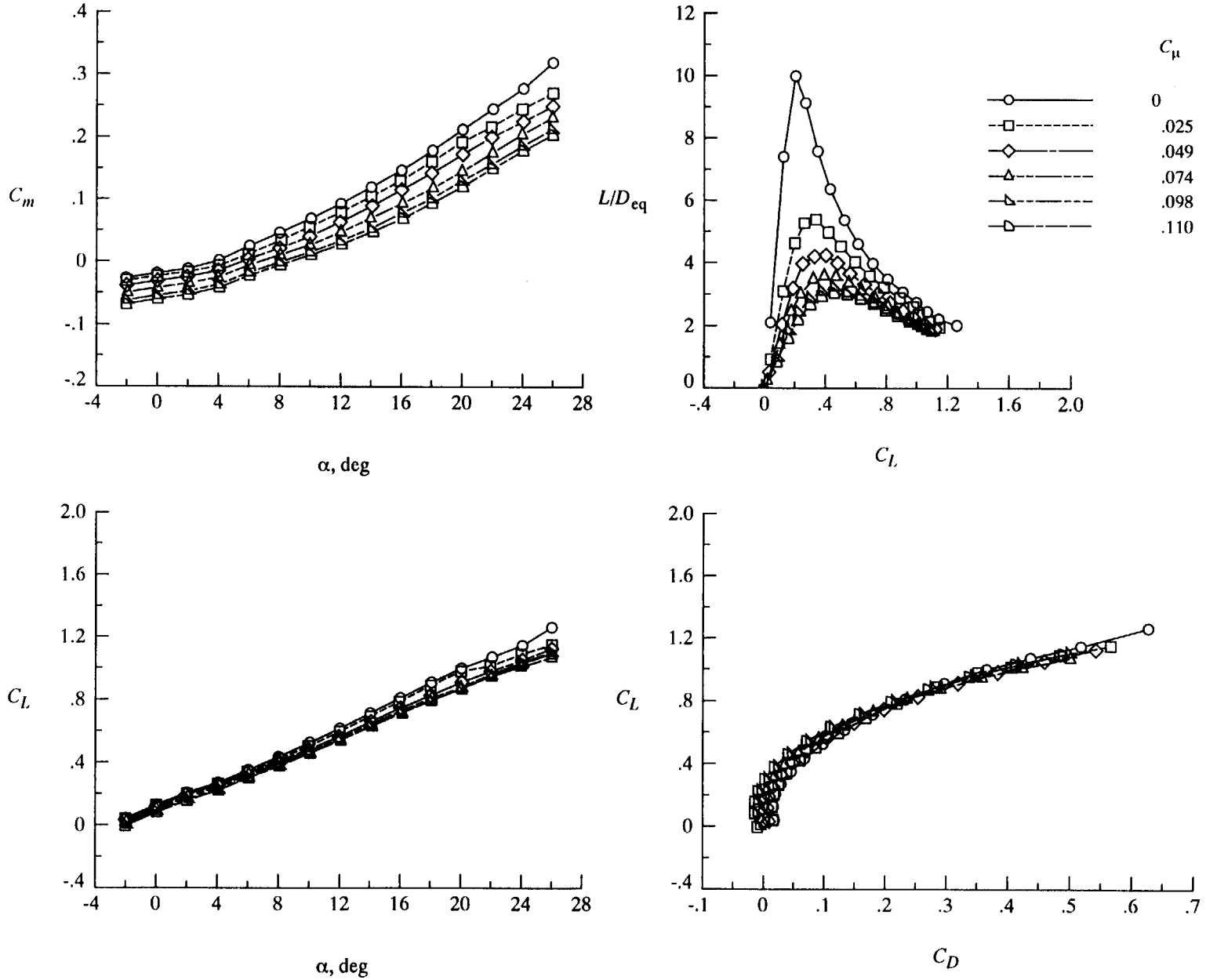

Figure 25. Effect of blowing coefficient on longitudinal aerodynamics of high-lift wing. Thrust included and q_∞ = 20 psf.

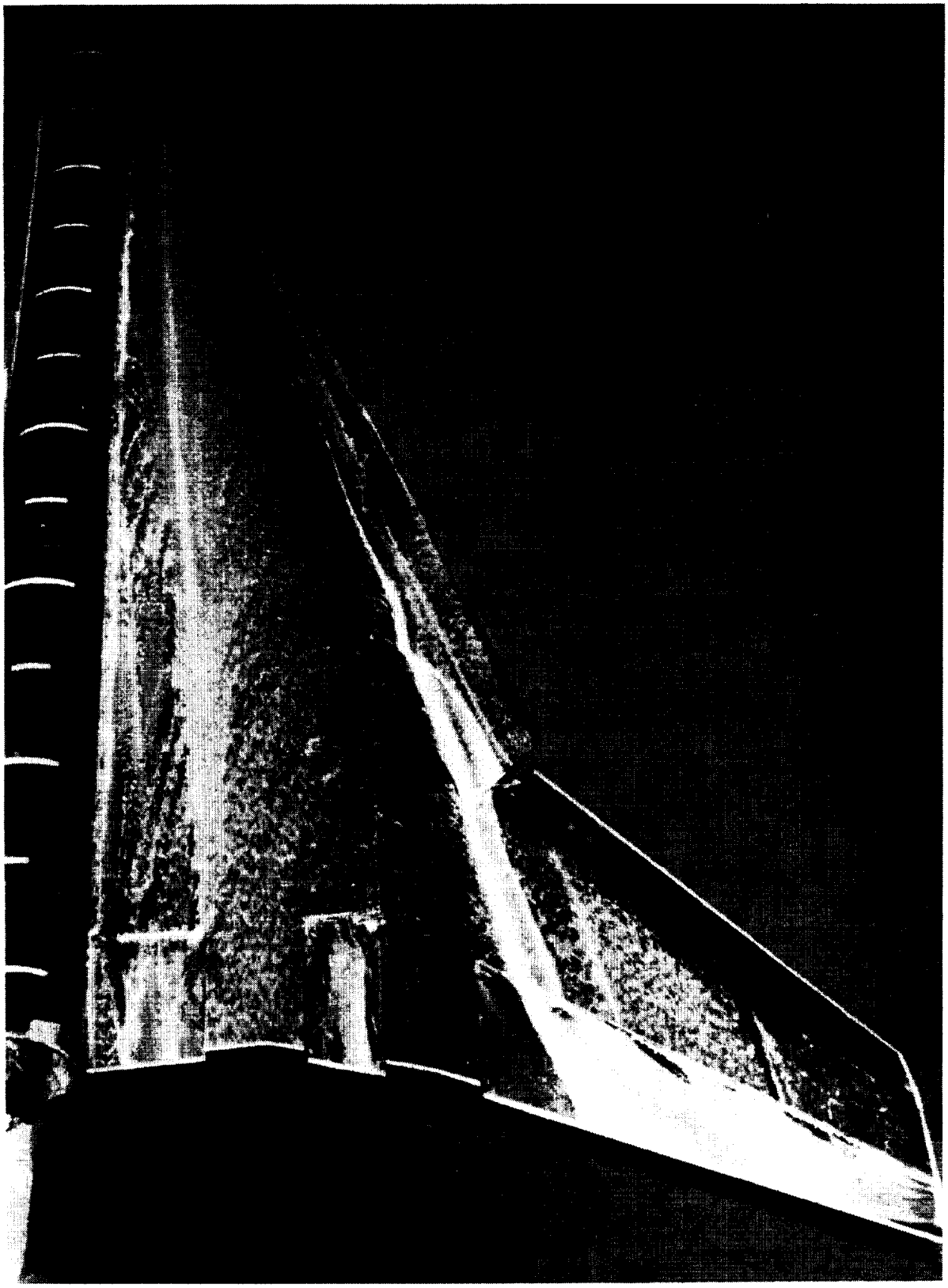

Figure 26. Surface flow visualization of high-lift wing. $\alpha = 10°$; $C_\mu = 0$; and $q_\infty = 35$ psf.

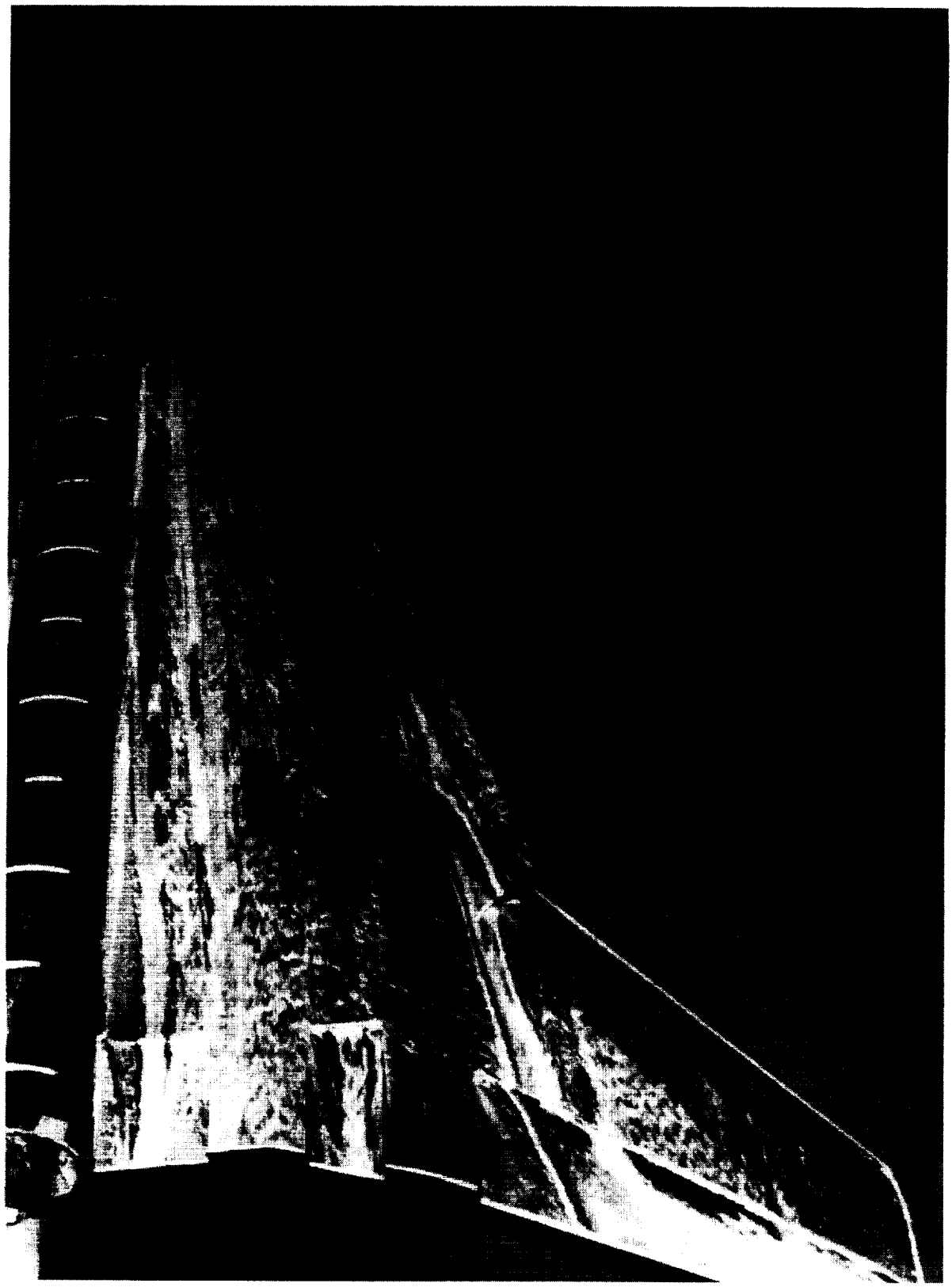

Figure 27. Surface flow visualization of high-lift wing. $\alpha = 10°$; $C_\mu = 0$; and $q_\infty = 20$ psf.

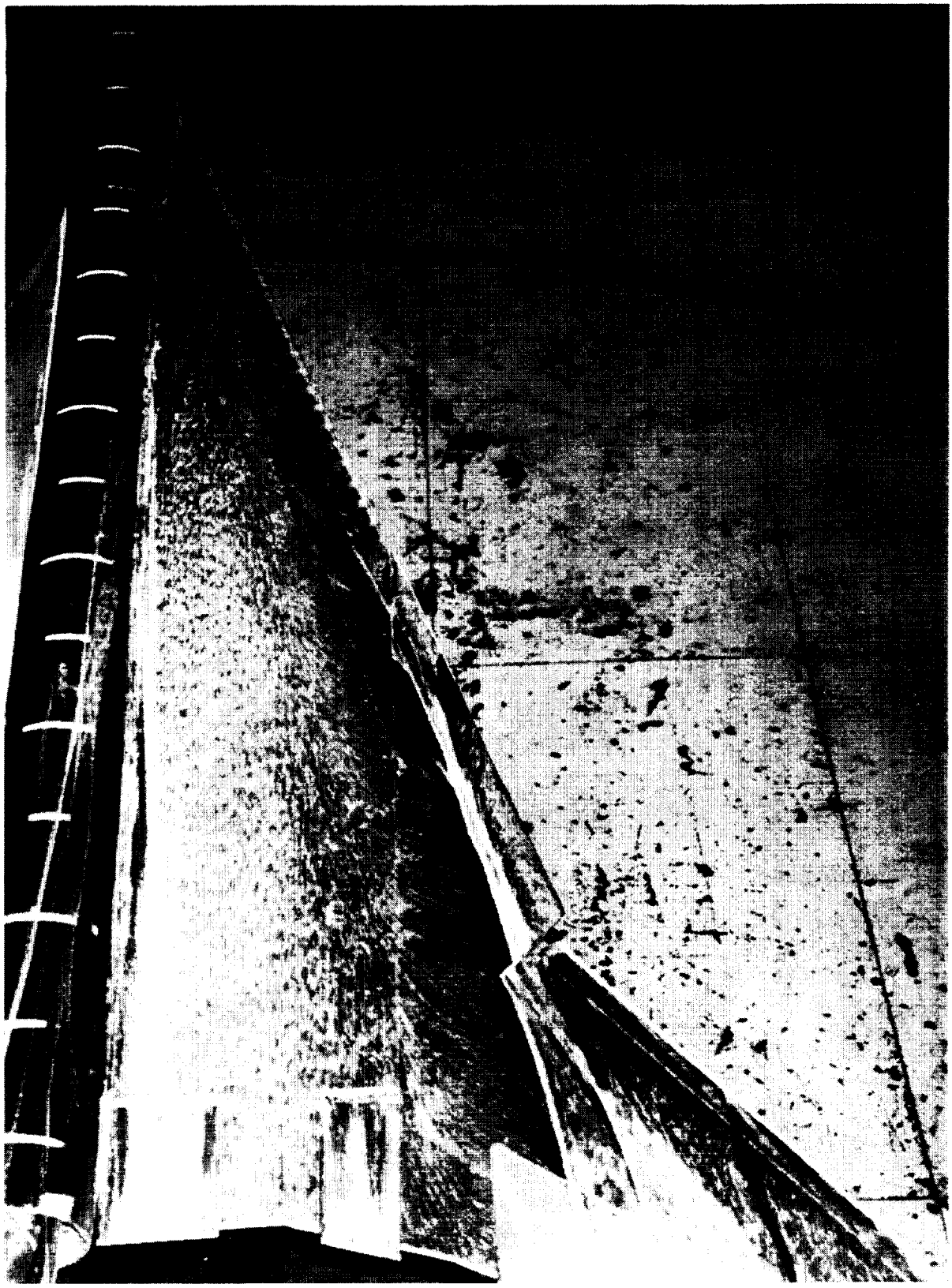

Figure 28. Surface flow visualization of high-lift wing. $\alpha = 10°$; $C_\mu = 0.015$; and $q_\infty = 35$ psf.

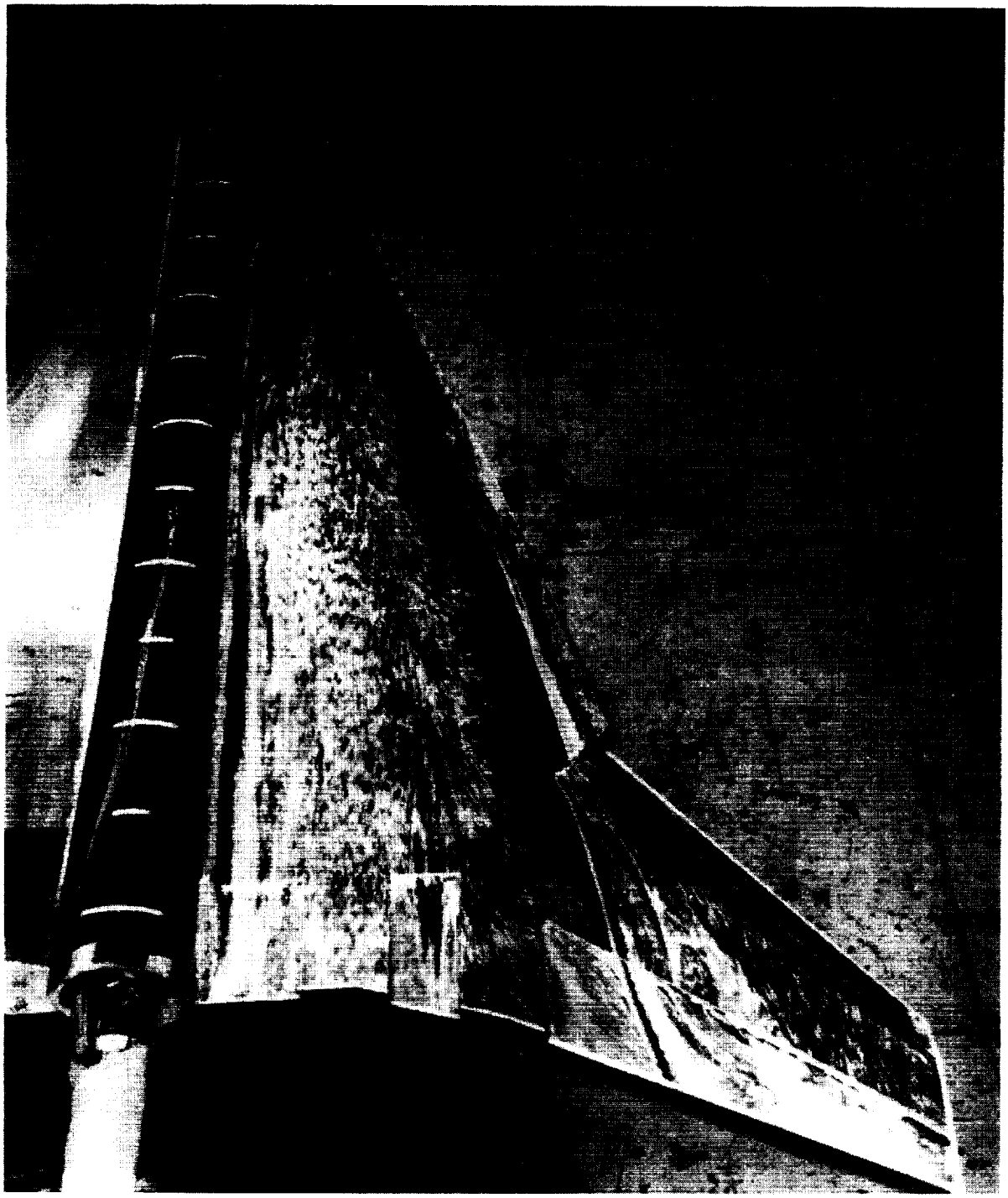

Figure 29. Surface flow visualization of high-lift wing. $\alpha = 10°$; $C_\mu = 0.025$; and $q_\infty = 20$ psf.

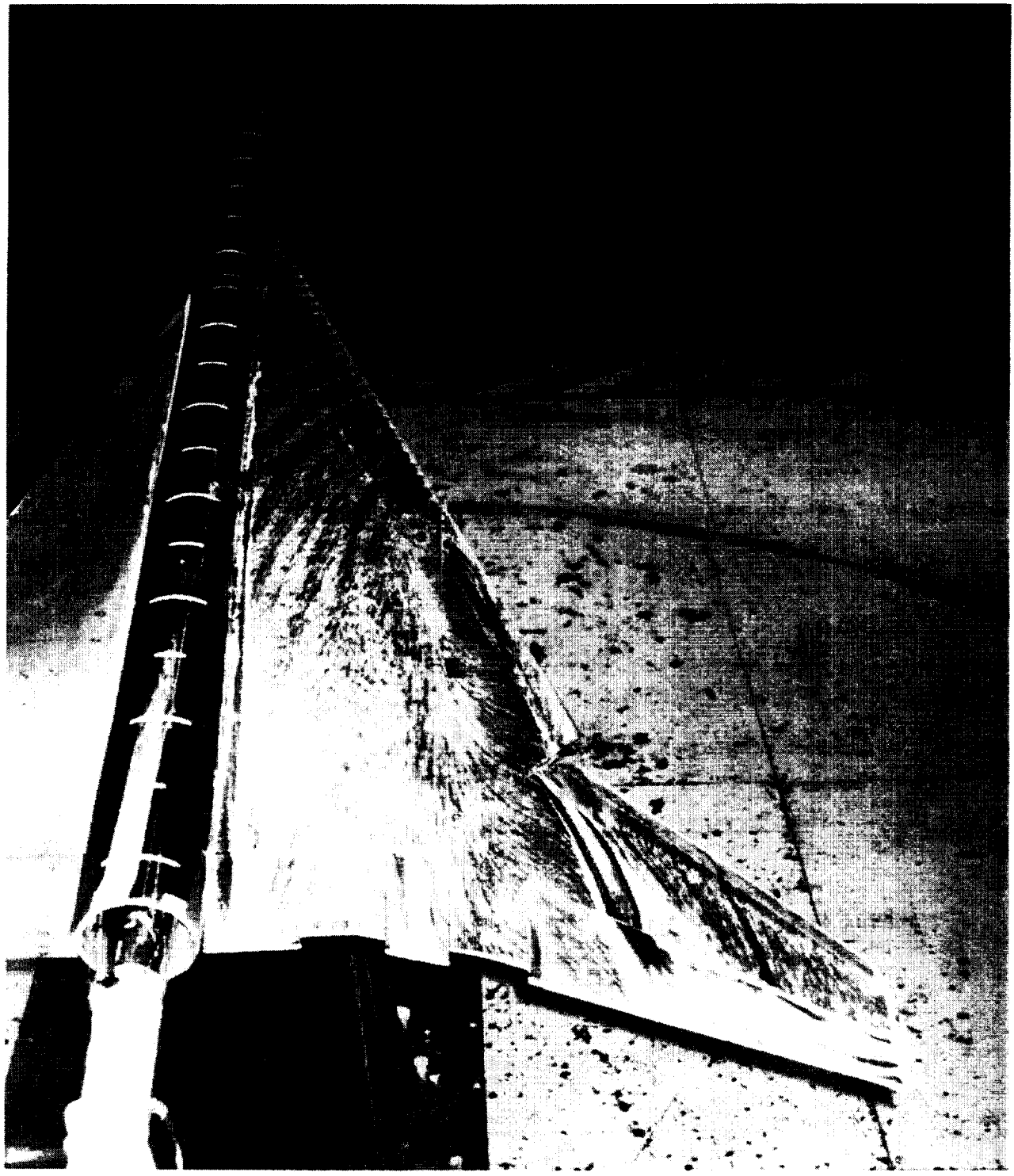

Figure 30. Surface flow visualization of high-lift wing. $\alpha = 10°$; $C_\mu = 0.050$; and $q_\infty = 20$ psf.

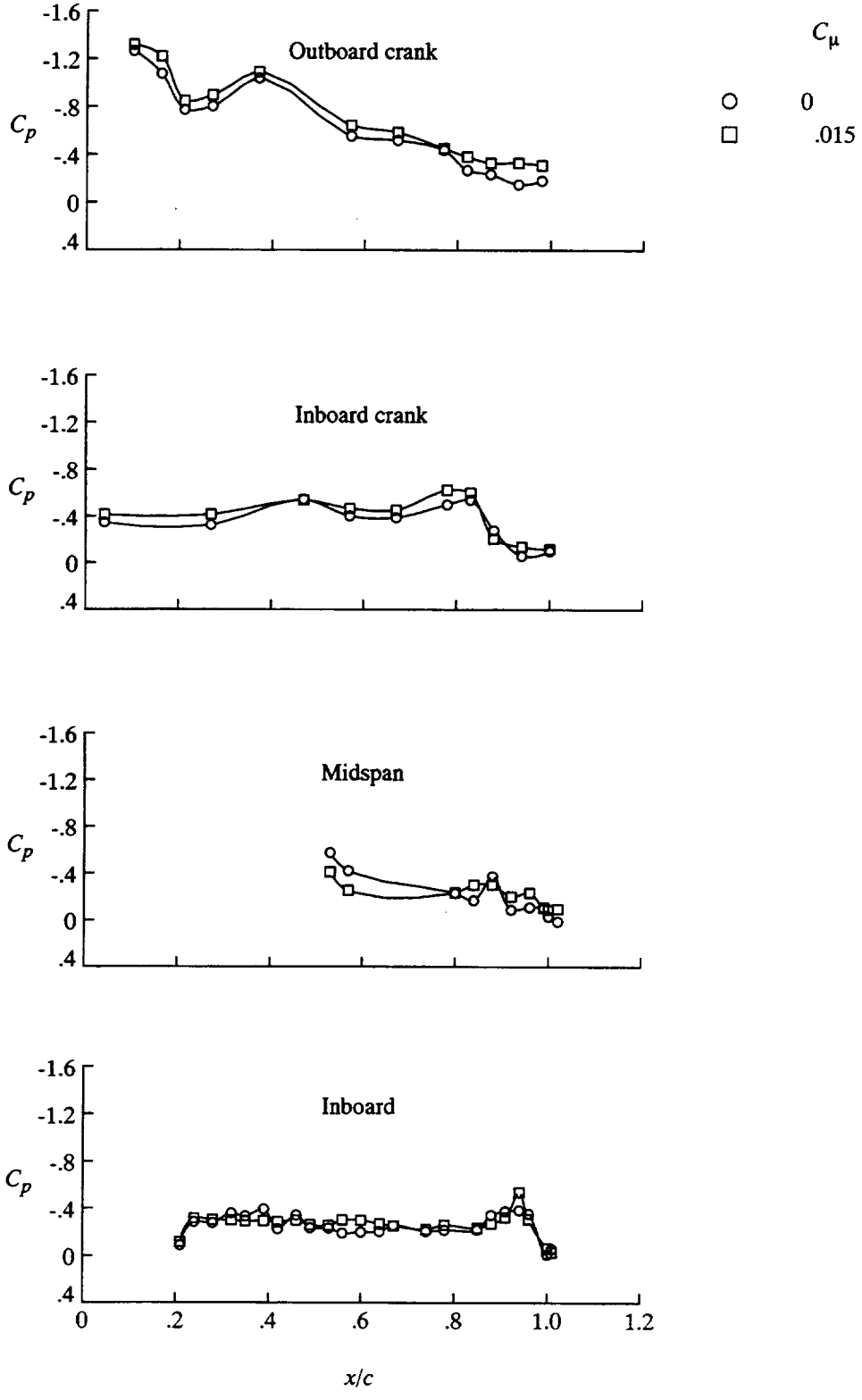

Figure 31. Effect of blowing coefficient on surface pressure distributions of high-lift wing. $\alpha = 10°$ and $q_\infty = 35$ psf.

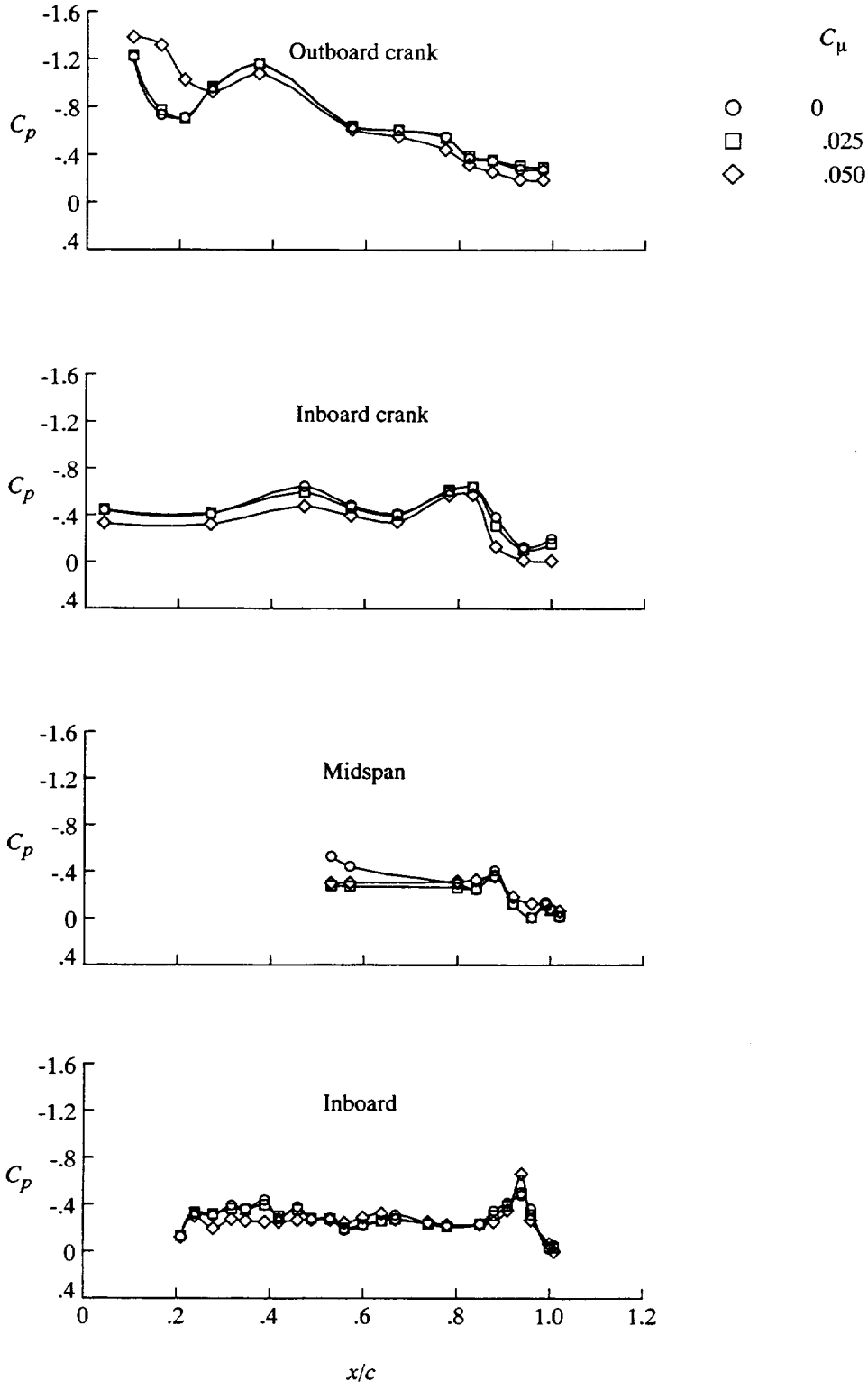

Figure 32. Effect of blowing coefficient on surface pressure distributions of high-lift wing. $\alpha = 10°$ and $q_\infty = 20$ psf.

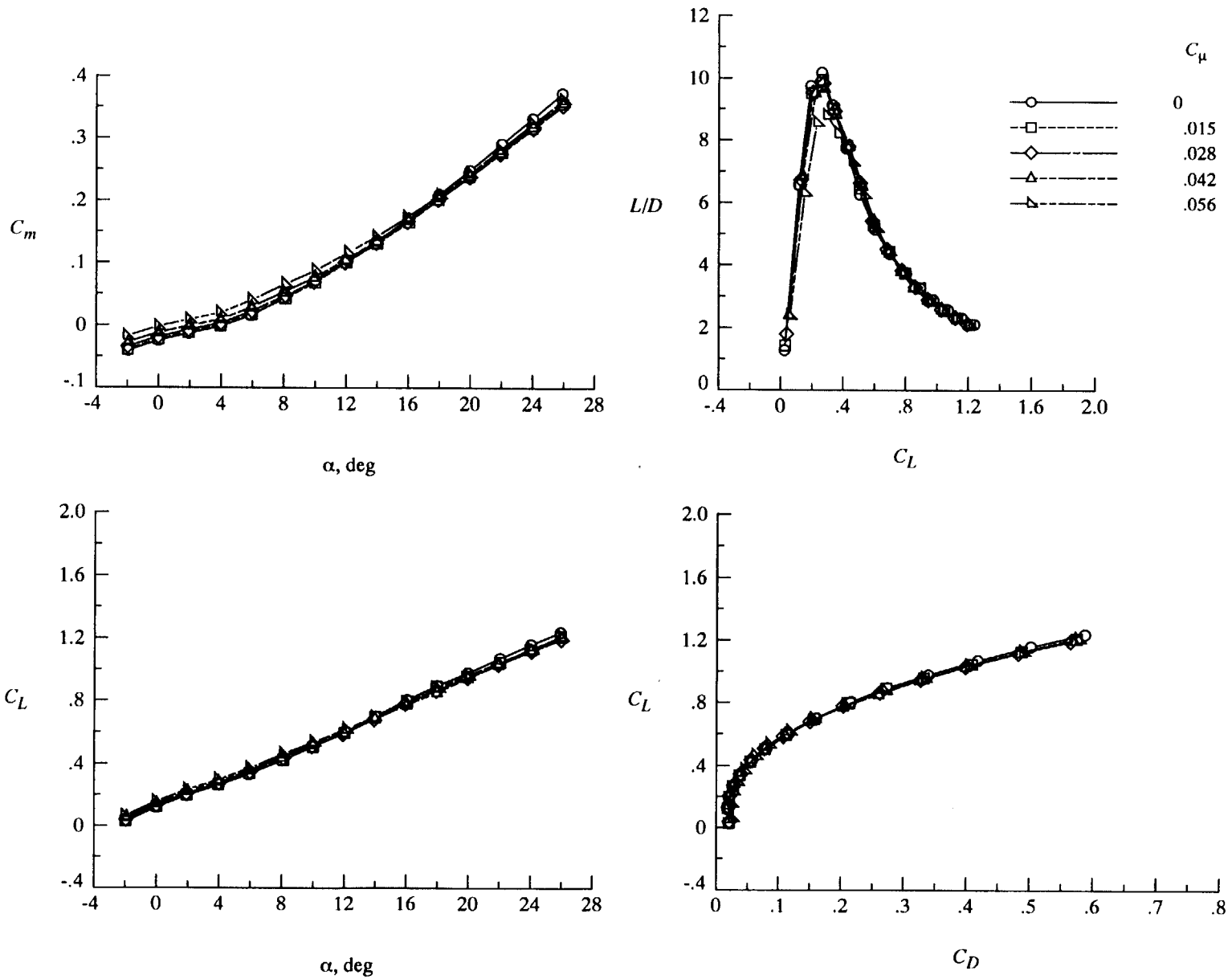

Figure 33. Effect of blowing coefficient on longitudinal aerodynamics of high-lift wing with Krueger flap. Thrust removed and q_∞ = 35 psf.

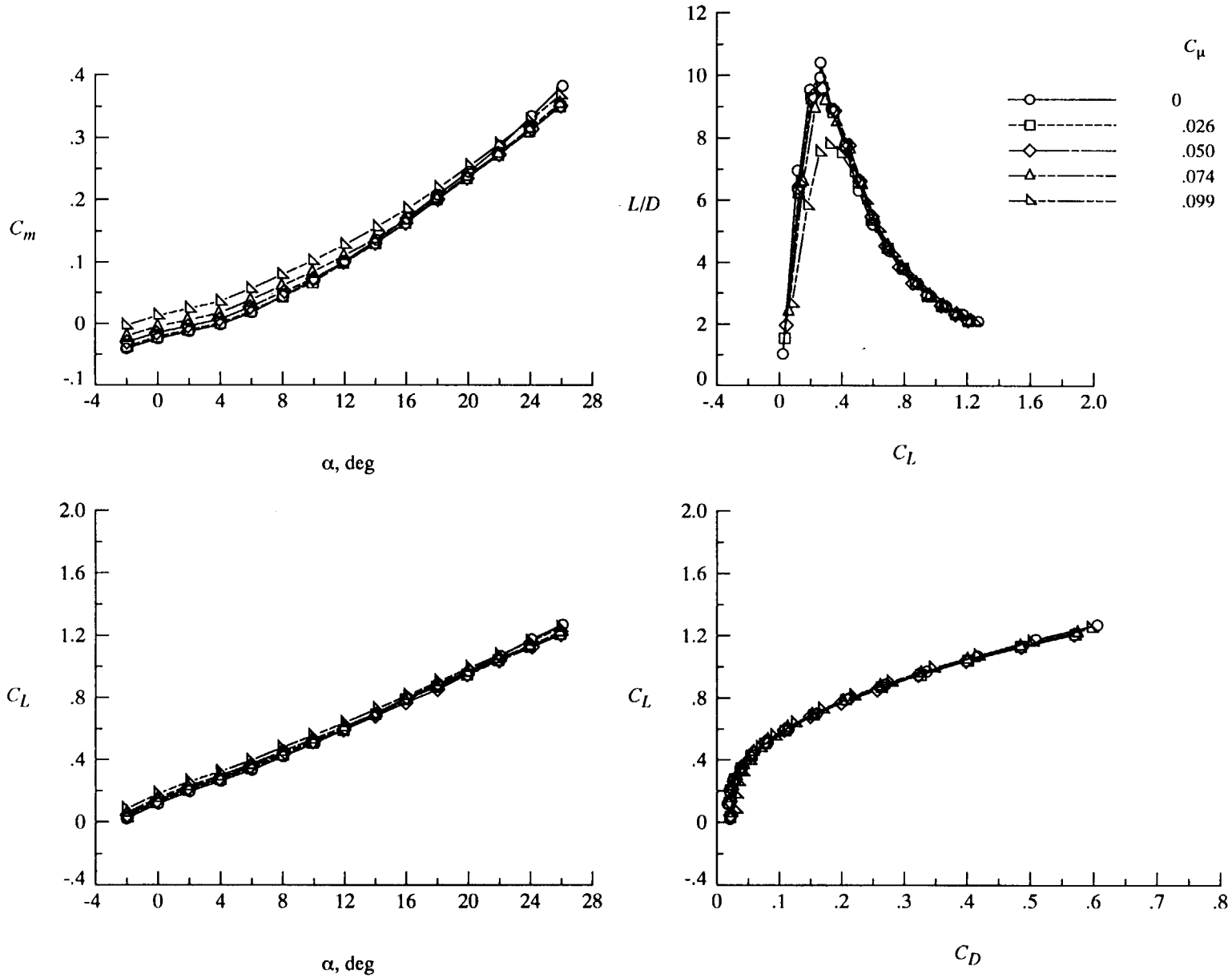

Figure 34. Effect of blowing coefficient on longitudinal aerodynamics of high-lift wing with Krueger flap. Thrust removed and q_∞ = 20 psf.

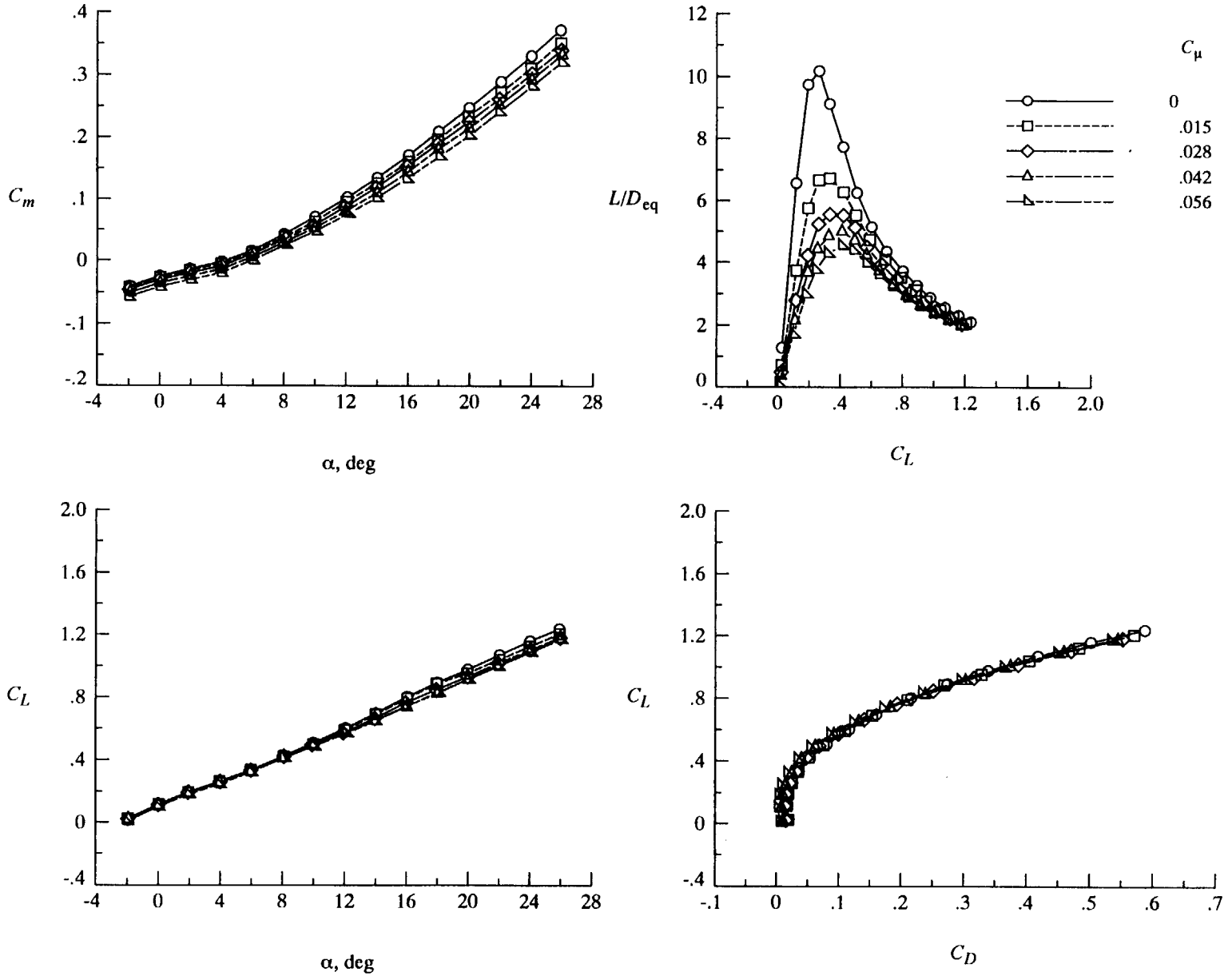

Figure 35. Effect of blowing coefficient on longitudinal aerodynamics of high-lift wing with Krueger flap. Thrust included and q_∞ = 35 psf.

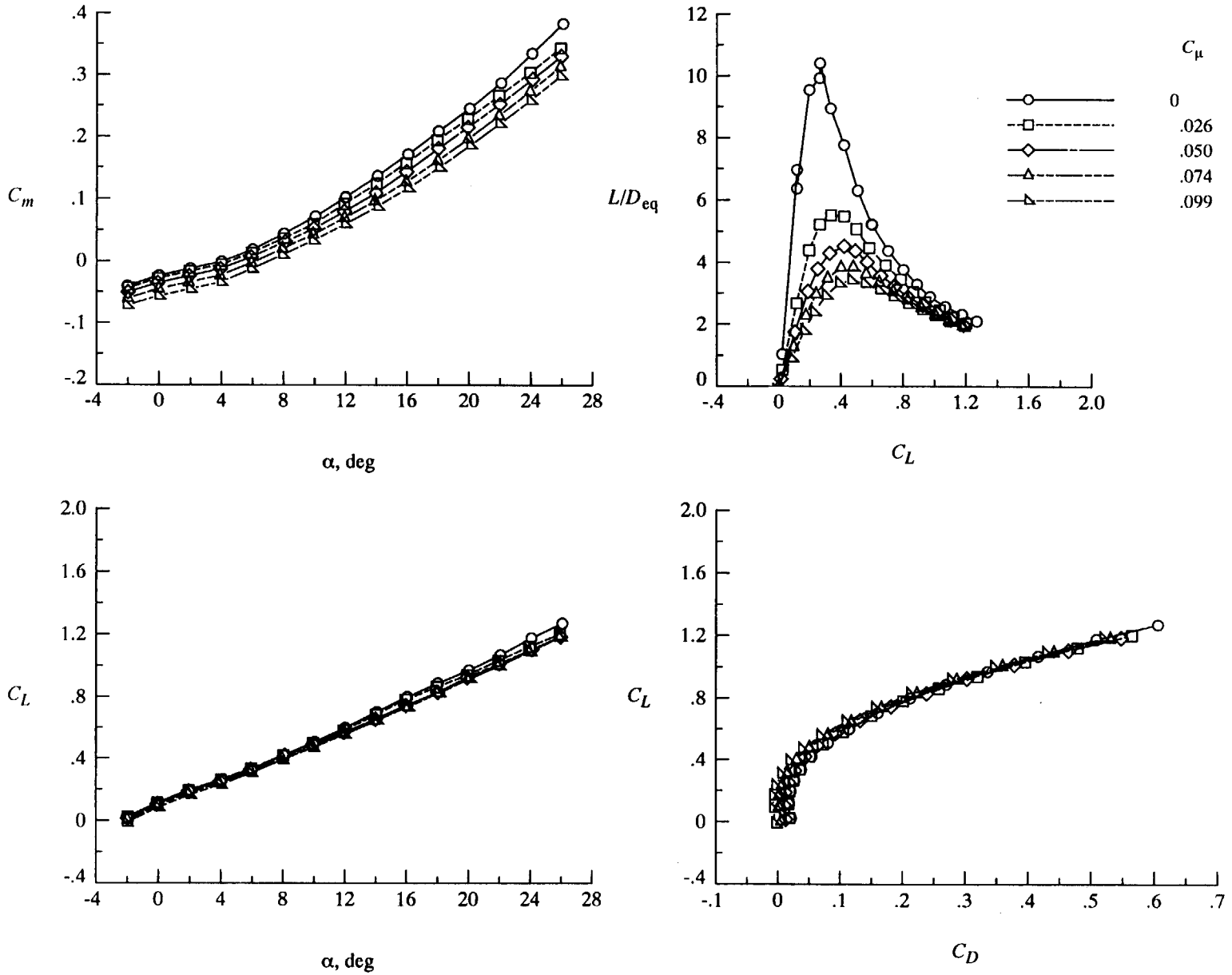

Figure 36. Effect of blowing coefficient on longitudinal aerodynamics of high-lift wing with Krueger flap. Thrust included and q_∞ = 20 psf.

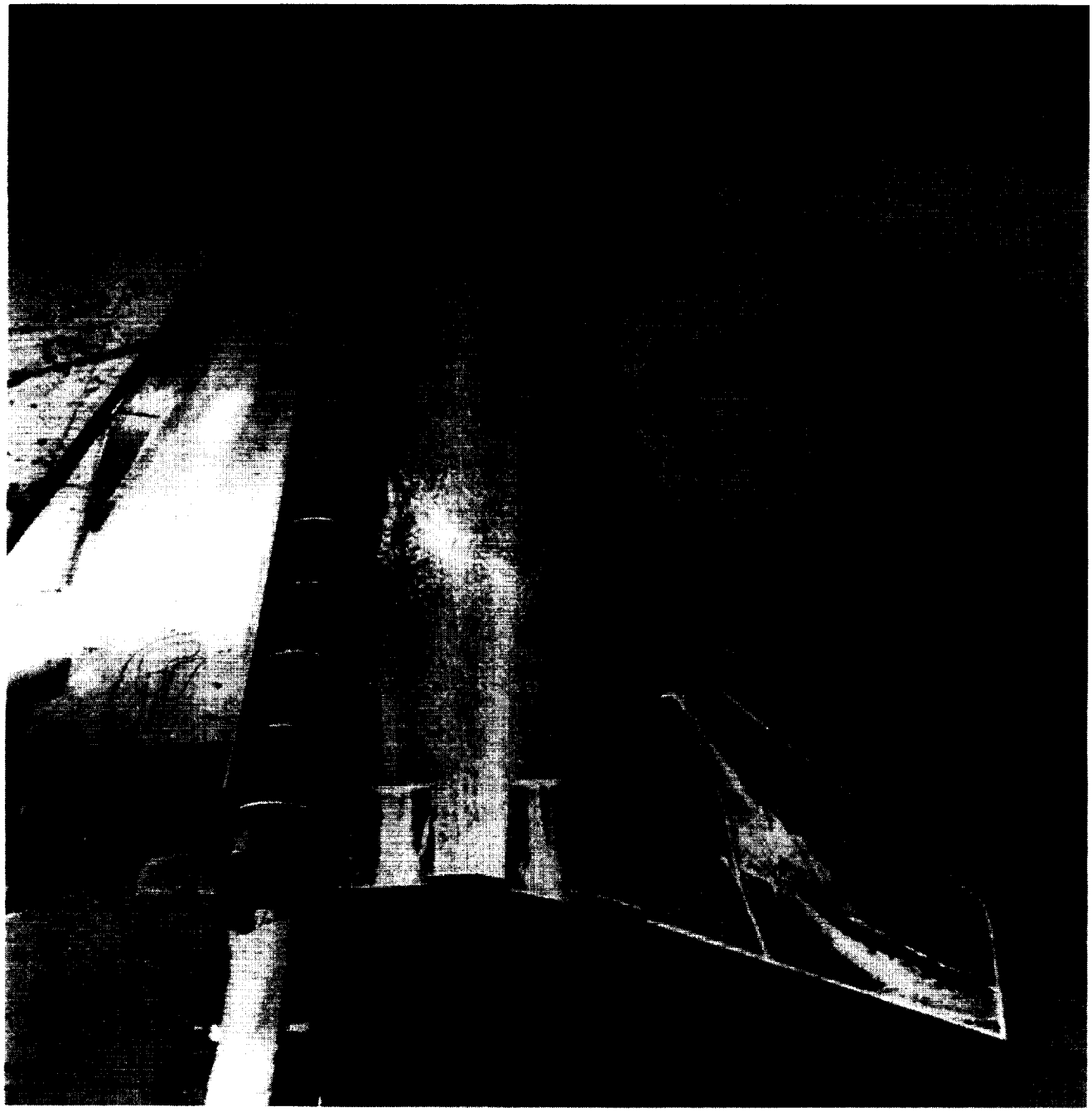

Figure 37. Surface flow visualization of high-lift wing with Krueger flap. $\alpha = 10°$; $C_\mu = 0$; and $q_\infty = 20$ psf.

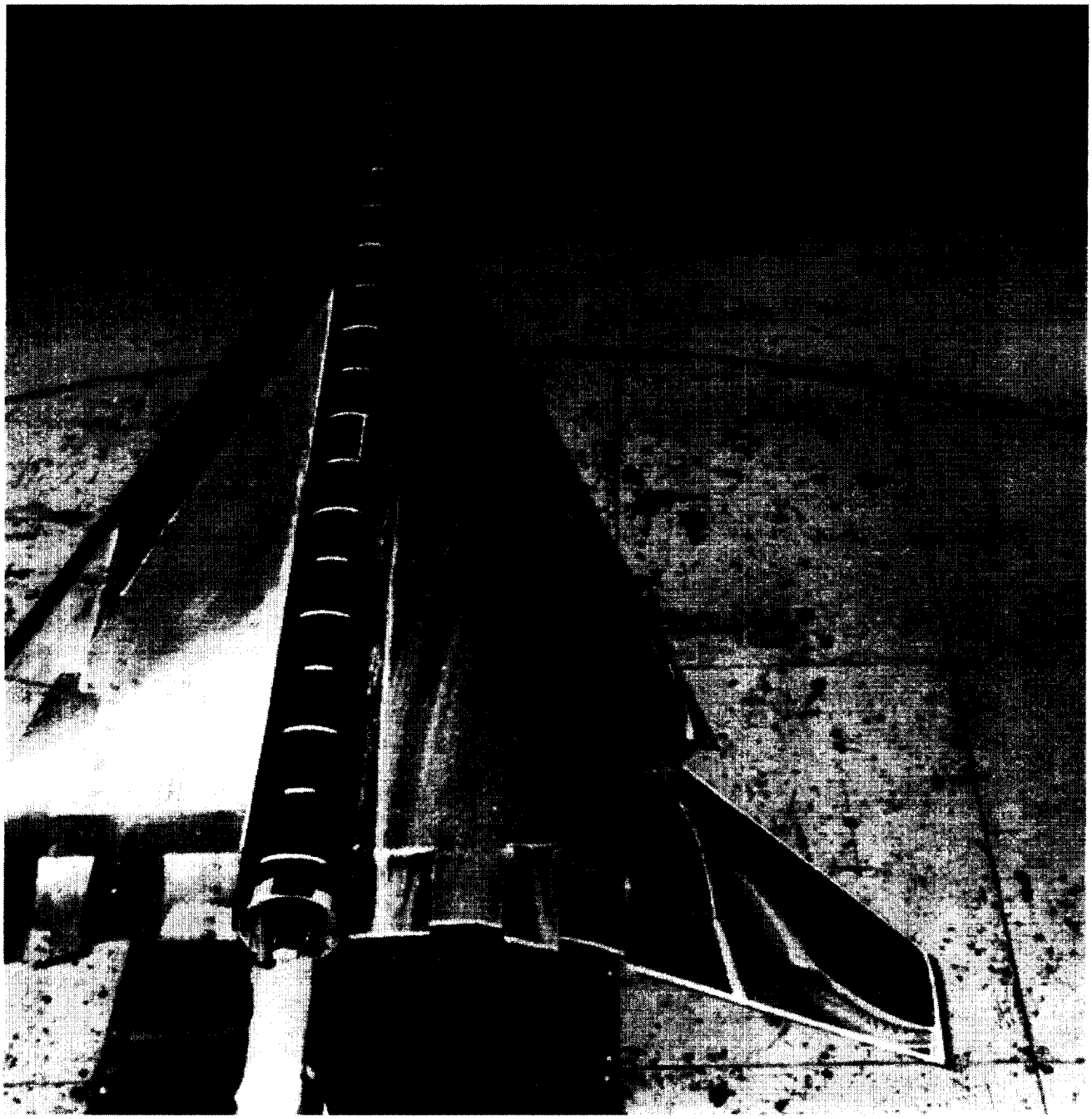

Figure 38. Surface flow visualization of high-lift wing with Krueger flap. $\alpha = 10°$; $C_\mu = 0.026$; and $q_\infty = 20$ psf.

Figure 39. Surface flow visualization of high-lift wing with Krueger flap. $\alpha = 10°$; $C_\mu = 0.050$; and $q_\infty = 20$ psf.

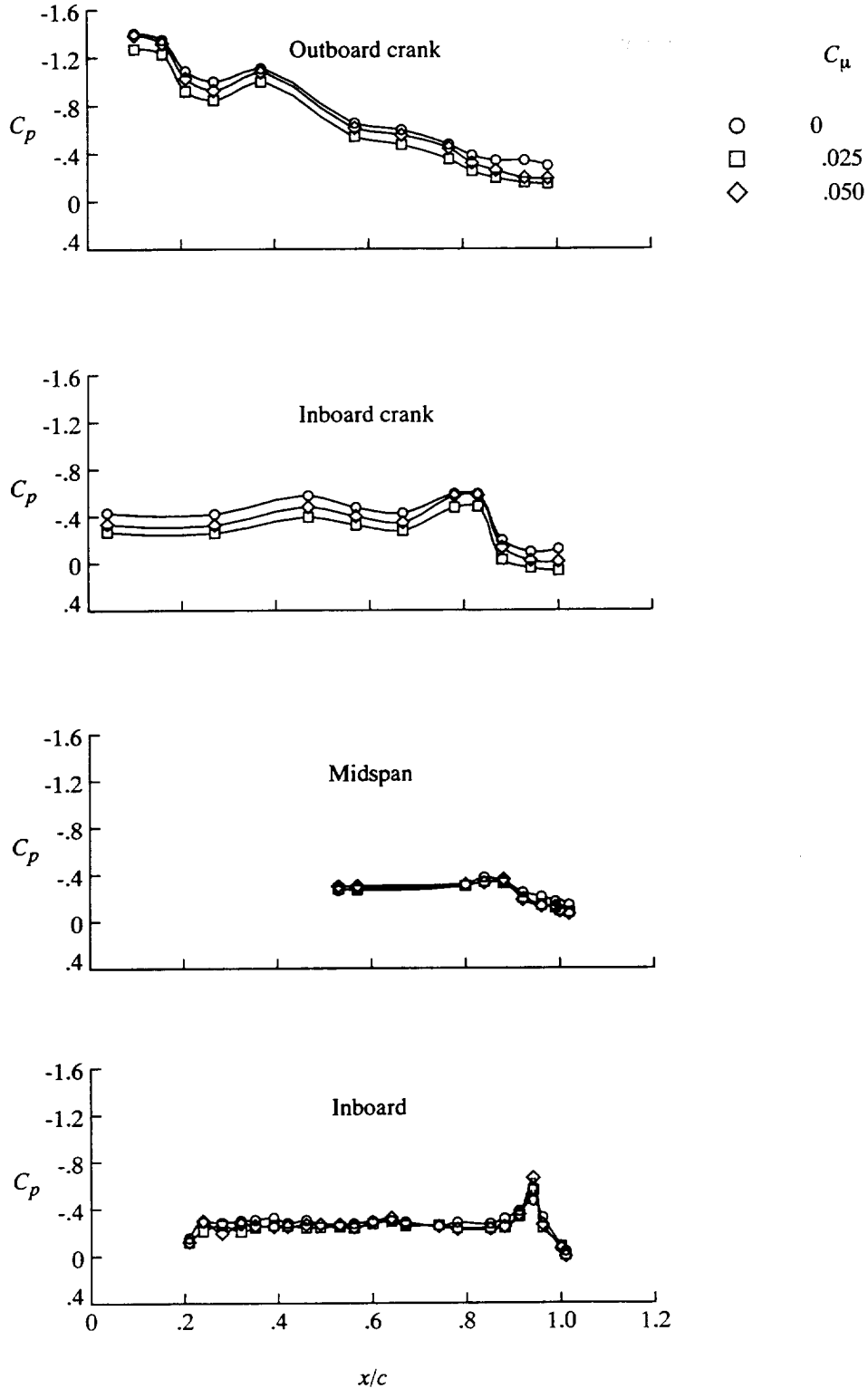

Figure 40. Effect of blowing coefficient on surface pressure distributions of high-lift wing with Krueger leading-edge flap. $\alpha = 10°$ and $q_\infty = 20$ psf.

REPORT DOCUMENTATION PAGE

Form Approved
OMB No. 0704-0188

1. AGENCY USE ONLY *(Leave blank)*	2. REPORT DATE	3. REPORT TYPE AND DATES COVERED
	December 1999	Technical Publication

4. TITLE AND SUBTITLE
Low-Speed Investigation of Upper-Surface Leading-Edge Blowing on a High-Speed Civil Transport Configuration

5. FUNDING NUMBERS
WU 537-03-22-02

6. AUTHOR(S)
Daniel W. Banks, Brenda E. Gile Laflin, Guy T. Kemmerly, and Bryan A. Campbell

7. PERFORMING ORGANIZATION NAME(S) AND ADDRESS(ES)
NASA Langley Research Center
Hampton, VA 23681-2199

8. PERFORMING ORGANIZATION REPORT NUMBER
L-17483

9. SPONSORING/MONITORING AGENCY NAME(S) AND ADDRESS(ES)
National Aeronautics and Space Administration
Washington, DC 20546-0001

10. SPONSORING/MONITORING AGENCY REPORT NUMBER
NASA/TP-1999-209538

11. SUPPLEMENTARY NOTES

12a. DISTRIBUTION/AVAILABILITY STATEMENT
Unclassified–Unlimited
Subject Category 02 Distribution: Nonstandard
Availability: NASA CASI (301) 621-0390

12b. DISTRIBUTION CODE

13. ABSTRACT ***(Maximum 200 words)***
An exploratory investigation of the effectiveness of upper-surface leading-edge blowing on a High-Speed Civil Transport (HSCT) configuration was conducted in the Langley 14- by 22-Foot Subsonic Tunnel. The objective of the investigation was to determine how effective upper-surface leading-edge blowing is for increasing lift and lift-drag ratios for an HSCT-class airplane at takeoff, initial climb, and approach to landing. The research was conducted on a modified model of a generic HSCT configuration. The model geometry included a cranked delta wing with an inboard sweep of 71°, an outboard sweep of 50°, and a relatively thin airfoil section. Because the leading edge was thin, the blowing slot, unlike conventional leading-edge blowing tangent to the leading edge, was behind the leading edge and blowing tangent to the upper surface. Furthermore, because of fabrication constraints, the blowing slot was located only on the inboard two-thirds of the wing 71°-sweep leading edge. Results indicate that this type of blowing at the test conditions was able to modify the local flow structure; however, it had little beneficial effects on overall lift and drag characteristics.

14. SUBJECT TERMS	15. NUMBER OF PAGES
HSCT; HSR; High lift; Leading-edge blowing; Vortical flow	62
	16. PRICE CODE: A04

17. SECURITY CLASSIFICATION OF REPORT	18. SECURITY CLASSIFICATION OF THIS PAGE	19. SECURITY CLASSIFICATION OF ABSTRACT	20. LIMITATION OF ABSTRACT
Unclassified	Unclassified	Unclassified	UL